An analytical model for solute transport in unsaturated flow through a single fracture and porous rock matrix

J. E. Houseworth

Lawrence Berkeley National Laboratory, Berkeley, California, USA

Received 27 October 2004; revised 26 September 2005; accepted 24 October 2005; published 27 January 2006.

[1] An exact analytical solution is presented for solute transport in an unsaturated, vertical fracture and porous rock matrix. The problem includes advective transport in the fracture and rock matrix as well as advective and diffusive fracture-matrix exchange. Linear sorption and radioactive decay are also treated. The solution is derived under the assumptions that longitudinal diffusion and dispersion are negligible and that the fracture and rock properties are homogeneous. The water flux and saturation within the matrix are assumed to be steady and spatially uniform. The fracture flux, saturation, and wetted fracture-matrix interface area are steady but are allowed to be spatially variable. The problem is first solved in terms of solute concentrations that result from an instantaneous point source in the fracture. An integrated form of the solution is also derived for cumulative solute mass flux at a fixed downstream position. The closed-form analytical solution is expressed in terms of algebraic functions, exponentials, and error functions. Analyses indicate limited sensitivity to fracture porosity and fracture retardation under typical conditions but strong sensitivity to matrix diffusion, matrix retardation, and matrix imbibition.

Citation: Houseworth, J. E. (2006), An analytical model for solute transport in unsaturated flow through a single fracture and porous rock matrix, *Water Resour. Res.*, *42*, W01416, doi:10.1029/2004WR003770.

1. Introduction

[2] Transport in fractured rock typically results from a combination of relatively fast transport in fractures coupled with much slower transport in the rock matrix. Fracture pathways often carry most of the flow but have relatively small water content; therefore transport velocities in fractures are high. The rock matrix lying between fractures often carries a smaller fraction of the total flow, but is dominant in terms of water content, leading to much lower transport velocities. Transport through saturated fractured rock was investigated in analytical models by *Neretnieks* [1980], *Tang et al.* [1981], *Sudicky and Frind* [1982], and *Maloszewski and Zuber* [1985]. Although complete water saturation is not a strict requirement for the application of these models, they are limited to diffusive exchange between fractures and matrix, with no flow in the matrix. Existing analytical models for transport through fractured rock have not addressed the effects of advective exchange between the fracture and the rock matrix, nor the effects of global advective transport through the rock matrix. The model presented here addresses these transport processes.

[3] Flow in the rock matrix results from both capillary and gravity forces. In unsaturated fractured rock systems, advective transport between the fractures and matrix may occur as a result of flow driven by differences in capillary pressure. Such effects have been noted to result in slower transport because capillary pressure conditions typically lead to flow from the fractures to the matrix [*Ho*, 2001]. On the other hand, advection through the matrix in the direction of the mean flow will facilitate overall transport. Therefore advection in the matrix can affect solute transport in qualitatively different ways.

[4] Although transport through a single fracture in a porous rock is a highly idealized representation of a fractured rock, it has been found to be useful for interpretation of laboratory and field data in saturated zone environments [*Maloszewski and Zuber*, 1985, 1990, 1993; *Becker and Shapiro*, 2000; *Shapiro*, 2001]. The effects of multiple fractures may be neglected for cases in which the timescale for advection in the fracture across the model domain is short in comparison with the timescale for lateral migration between flowing fractures.

[5] Beyond direct application to physical systems, analytical models provide a way to test and develop numerical models. Currently, there are no analytical models available for testing numerical models of systems in which advective transport occurs in both the fractures and matrix, as in a dual-permeability model. Furthermore, analytical models may serve as a component of a numerical model to improve the accuracy and efficiency of the numerical model [*Pan and Bodvarsson*, 2002; *Robinson et al.*, 2003; *Zimmerman et al.*, 1996].

[6] The model presented here includes three independent velocities; a longitudinal velocity in the fracture, a longitudinal velocity in the matrix, and a transverse velocity between the fracture and matrix. The model also treats diffusive solute exchange between the fracture and matrix, linear sorption in the fracture and matrix, and radioactive

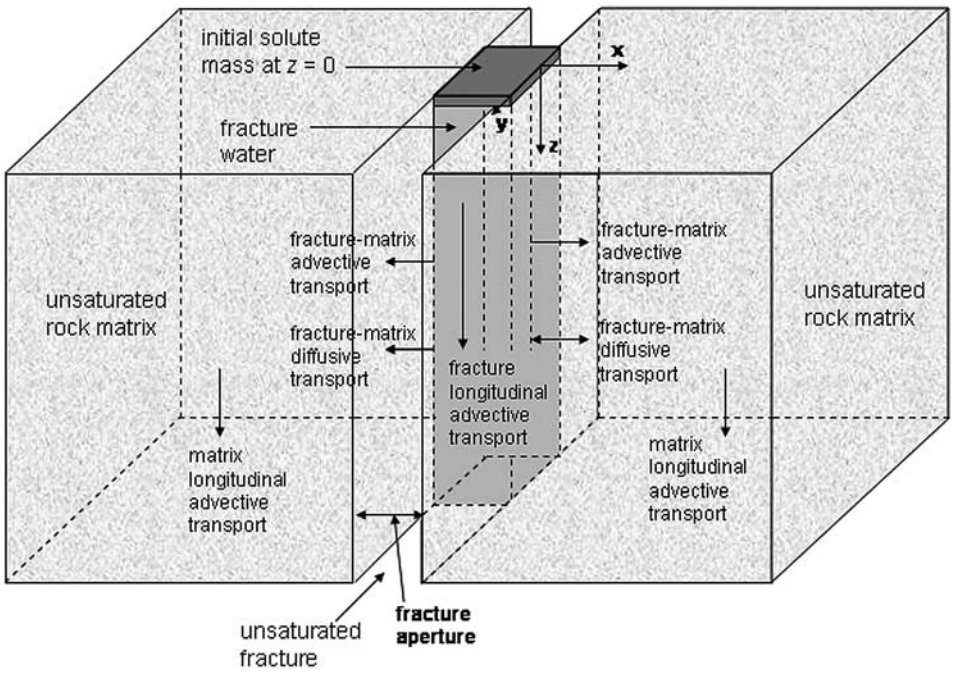

Figure 1. Schematic diagram of transport processes and solute source configuration in the single-fracture model.

decay. Figures 1 and 2 provide schematic diagrams for the model. Figure 1 shows the main transport mechanisms of longitudinal advection in the fracture and matrix and advective and diffusive exchange between the fracture and matrix for an initial solute source in the fracture. Imbibition of water from the fracture to the matrix causes changes in the fracture flow pattern as indicated in Figure 2. Figure 2 presents a view in the plane of the fracture. The conceptual model for water flow in a vertical fracture is based on a channelized flow pattern that results from flow instability. Unstable flow patterns have been observed in laboratory experiments of flow in vertical fractures [*Glass et al.*, 1995; *Nicholl et al.*, 1994] and in numerical models of such processes [*Hughes and Blunt*, 2001]. Channels with low flux do not span the vertical dimension in Figure 2 because imbibition into the matrix eliminates these channels before reaching the lower boundary. For cases without imbibition flow, all channels span the domain. Regions in the rock matrix that connect with fracture water through movement in the x direction only are referred to here as the connected matrix. The remaining regions of the matrix are referred to as the isolated matrix. Note that as imbibition of water

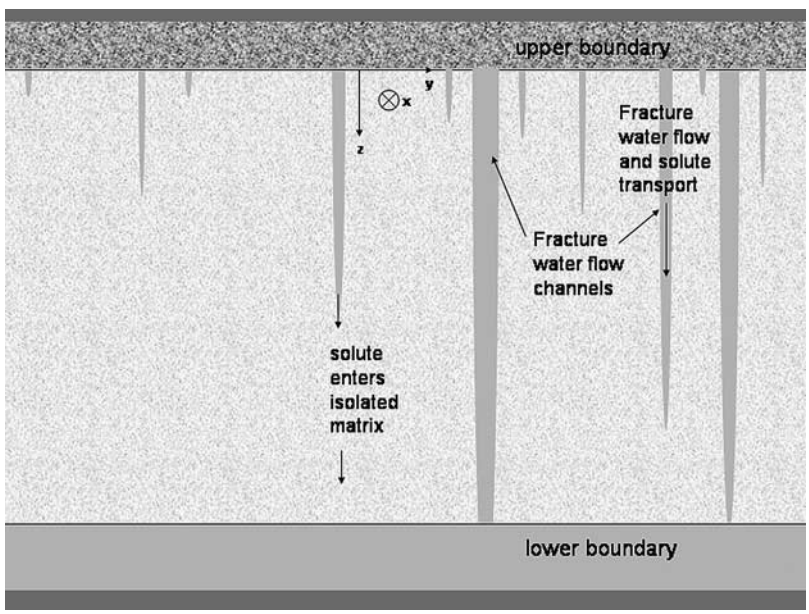

Figure 2. Schematic diagram of fracture flow channels in the fracture plane, the associated fracture-matrix contact area, and transport in the fracture plane and rock matrix.

occurs, fracture water saturation is reduced. Continued solute movement in the vertical direction through the connected matrix leads to solute transport through the isolated matrix (Figure 2).

[7] The model presented here is restricted to the following assumptions.

[8] 1. Steady flow in the fracture and rock matrix.

[9] 2. Water flux in the fracture is proportional to the water saturation.

[10] 3. Wetted fracture-matrix interface area is proportional to the water saturation.

[11] 4. Semi-infinite domain longitudinally and infinite domain laterally.

[12] 5. Vertical (longitudinal) diffusion and dispersion are negligible.

[13] 6. Horizontal advective and diffusive transport parallel to the fracture plane is negligible.

[14] 7. Velocity in the fracture is larger than the longitudinal velocity in the matrix.

[15] 8. Transverse diffusive mixing normal to the fracture wall maintains a uniform solute concentration in fracture water at a given elevation.

[16] 9. Saturation variations in the matrix required to drive cross flow are sufficiently small such that they have a negligible effect on transport velocities in the transverse direction.

[17] Assumptions 1 and 2 are needed to simplify the flow problem sufficiently for analytical treatment of the transport problem. Steady state flow conditions may be found in unsaturated rock underlying a porous rock or soil zone with sufficient storage capacity to damp out transient infiltration from the ground surface [*Bodvarsson et al.*, 1999]. Imbibition flow between the fracture and rock matrix is idealized as flow driven by a uniform capillary pressure gradient laterally across the matrix. A direct proportionality between water flux in the fracture and fracture saturation is expected if capillary pressure forces in the fracture are small compared with gravitational forces. This relationship between water flux and saturation has been postulated for unsaturated flow in a vertical fracture [*Glass et al.*, 1995]. Assumption 3 is a hypothesis proposed by *Liu et al.* [1998] for fracture networks to account for changes in fracture-matrix interface area with changes in fracture saturation. Observations of unsaturated flow in a vertical fracture have demonstrated that the wetted interface area can be significantly less than the geometric interface area [*Glass et al.*, 2002]. Assumption 4 concerning the problem's geometry is also needed to specify and simplify the problem for analytical treatment. Longitudinal dispersion is neglected, as stated in assumption 5, to simplify the problem. The neglect of longitudinal diffusion and dispersion will lead to higher predicted solute concentrations. However, this is expected to be a good approximation for cases with sufficient fracture-matrix interaction [*Maloszewski and Zuber*, 1992]. Assumption 6 is needed to simplify the problem because of the complex nature of the distribution of flow channels in a fracture. For cases without imbibition, this assumption restricts solute to stay in the connected regions; diffusion into the isolated regions is neglected. For cases with imbibition, this assumption also restricts solute that advects into the isolated regions to remain in the isolated regions. This assumption will lead to higher predicted solute concentrations. However, the effects on longitudinal mass flux are not expected to be significant because of the secondary influence of transport parallel to the fracture plane on fracture-matrix exchange. Assumption 7 is generally true if fracture flow is a significant factor in the system. Assumption 8 is also generally true because diffusion across a dimension characterized by the fracture aperture will homogenize solute concentrations rapidly compared with other timescales associated with solute transport. Assumption 9 is based on the premise that imbibition cross flow in the matrix is small compared with the larger-scale flow in the vertical direction. Furthermore, the capillary pressure gradient required to drive this flow results in small changes in water saturation that have only a small effect on transverse transport velocities.

[18] As shown in Figure 2, there are three distinct flow domains for any given vertical trace between the upper boundary and the lower boundary: (1) fracture flow at the upper boundary penetrates to the lower boundary, (2) fracture flow at the upper boundary does not penetrate to the lower boundary because of matrix imbibition, and (3) no fracture flow between the upper and lower boundaries. According to assumption 6, transport is treated as a two-dimensional process in the x-z plane with no transport in the third (y) dimension. Furthermore, solute is introduced in the fracture flow exclusively. Therefore the third flow domain does not participate in the transport process. The first two flow domains do participate in the transport process. When fracture flow penetrates from the upper boundary to the lower boundary, solute is transported through flow in the fracture and the associated connected matrix. If fracture flow at the upper boundary does not penetrate to the lower boundary, solute introduced in the fracture flow at the upper boundary must pass through the isolated matrix to arrive at the lower boundary. There is a continuum of penetration depths for fracture flow between the upper and lower boundaries and the cumulative mass response for the isolated matrix accounts for this through integrating the responses over the range of penetration depths. Both domains must be addressed in the analysis of the cumulative mass arrivals at the lower boundary to account for all solute introduced at the upper boundary. The cumulative mass flux for the three three-dimensional problem is obtained through combining the two-dimensional solutions for the fracture and connected matrix (section 3.4) and the isolated matrix (section 3.5).

[19] Coupled transport equations for solute transport through the fracture and the rock matrix are developed in section 2. The coupling takes the form of a distributed source term in the conservation equation for the fracture and a boundary condition for the rock matrix. The two-dimensional transport problem in the rock matrix is reduced to a one-dimensional problem through a transformation to a coordinate system that moves at the longitudinal velocity in the rock matrix. The equations and boundary conditions are then transformed into dimensionless form. The solution for solute concentration from an instantaneous point source in the fracture is presented in sections 3.1, 3.2, and 3.3. Integrated forms of the solution representing the cumulative mass arrivals at a downstream location are derived in sections 3.4 and

3.5. Analyses conducted using the resulting solutions are presented in section 4.

2. Mathematical Formulation

2.1. Development of Conservation Equations

[20] The conservation equation for solute mass transport in a fracture is

$$\phi_f S_f \left(\frac{\partial c_f}{\partial t} + \lambda c_f\right) + A_r \rho_{bf} \left(\frac{\partial c_{fa}}{\partial t} + \lambda c_{fa}\right) + \frac{\partial (q_f c_f)}{\partial z} = A_{vfm} A_r \left(\phi_m S_m D_m \frac{\partial c_m}{\partial x}\bigg|_{x=0} - q_{fm} c_m|_{x=0}\right). \quad (1)$$

The first two terms on the left-hand side of equation (1) represent the rate of change in solute mass as a dissolved and sorbed species, respectively, including radioactive decay (see Notation section for a definition of mathematical terms). The third term represents the gradient in the advective solute mass flux through the fracture. The two terms on the right hand side of equation (1) represent the diffusive and advective exchange of solute mass between the fracture and the rock matrix. The fracture porosity allows for rock mass within the fracture volume.

[21] For a plane-parallel fracture, the fracture-matrix interface area for some representative fracture control volume is two times the fracture length (z direction) times the fracture depth (y direction). The fracture bulk volume for this same control volume is the fracture aperture, b, times the same length and depth. Therefore the fracture-matrix interface area per unit fracture volume is

$$A_{vfm} = \frac{2}{b}. \quad (2)$$

The fracture-matrix interface area per unit volume is multiplied by an area reduction factor, A_r. This factor is introduced to account for the reduction in fracture water contact with changes in fracture water saturation. Such a reduction factor has been postulated for unsaturated flow to account for effects such as flow instability, heterogeneity, and preferential flow [*Liu et al.*, 1998; *Doughty*, 1999].

[22] For a linear sorption process

$$c_{fa} = K_{df} c_f, \quad (3)$$

where K_{df} is the linear sorption coefficient in units of solution volume per unit rock mass.

[23] The Darcy flow rate in the fracture is q_f and the Darcy flow rate between the fracture and matrix is q_{fm}. A mass balance for water shows that

$$\frac{dq_f}{dz} = -\frac{2A_r q_{fm}}{b}. \quad (4)$$

Also note that $c_m|_{x=0} = c_f$.

[24] Using equations (2) through (4) in equation (1) gives

$$\frac{\partial c_{f\lambda}}{\partial t} + v_f \frac{\partial c_{f\lambda}}{\partial z} = \left(\frac{2A_r}{b}\right)\left(\frac{\phi_m S_m R_m}{\phi_f S_f R_f}\right)\left(D_m^* \frac{\partial c_{m\lambda}}{\partial x}\bigg|_{x=0}\right), \quad (5)$$

where

$R_f = 1 + \dfrac{A_r \rho_{bf} K_{df}}{\phi_f S_f}$ is the retardation coefficient in for transport in the fractures,

$v_f = \dfrac{q_f}{\phi_f S_f R_f}$ is the advective transport velocity in the fractures (z direction),

$v_{fm} = \dfrac{q_{fm}}{\phi_m S_m R_m}$ is the advective transport velocity in the matrix (x direction),

$D_m^* = \dfrac{D_m}{R_m}$ is the effective matrix diffusion coefficient,

$R_m = 1 + \dfrac{\rho_{bm} K_{dm}}{\phi_m S_m}$ is the retardation coefficient for transport in the matrix,

and $c_{f\lambda}$ and $c_{m\lambda}$ are the solute mass concentrations in the fracture and matrix waters, respectively, multiplied by the radioactive decay factor, $e^{\lambda t}$.

[25] Equation (4) indicates that q_f is a function of z. As discussed in section 1, the flux in the fracture is assumed to be proportional to the water saturation. Therefore equation (4) gives a relationship between S_f and z. A hypothesis proposed by *Liu et al.* [1998] is that the area reduction factor, A_r, is equal to the effective fracture saturation. For a residual saturation of zero, this hypothesis for the area reduction factor leads to the result that the group of factors multiplying the concentration gradient on the right hand side of equation (5) is constant. A related assumption is that the mass of rock available for sorption in the fracture per unit fracture volume is equal to the product of the bulk rock density in the fracture times the fraction of interface area that is wetted. This results in a constant retardation factor in the fracture for varying water saturation. Therefore the solute velocity in the fracture is constant.

[26] The conservation equation for solute mass transport in the rock matrix is

$$\phi_m S_m \left(\frac{\partial c_m}{\partial t} + \lambda c_m\right) + \rho_{bm} \left(\frac{\partial c_{ma}}{\partial t} + \lambda c_{ma}\right) + q_m \frac{\partial c_m}{\partial z} + q_{fm} \frac{\partial c_m}{\partial x} = \phi_m S_m D_m \frac{\partial^2 c_m}{\partial x^2}. \quad (6)$$

The first two terms on the left-hand side of equation (6) represent the rate of change in solute mass as a dissolved and sorbed species, respectively, including radioactive decay. The third and fourth terms represent the gradient in the advective solute mass flux through the matrix in the longitudinal and transverse directions, respectively. The term on the right hand side of equation (6) represents the gradient in the transverse diffusive flux through the rock matrix. Equation (6) only applies to the connected rock matrix that has a local contact with fracture water (see Figure 2). Transport in the isolated matrix, lacking a local contact with fracture water, is treated in section 3.3.

[27] For a linear sorption process,

$$c_{ma} = K_{dm} c_m, \quad (7)$$

where K_{dm} is the linear sorption coefficient in the rock matrix.

[28] Using equation (7) in equation (6) gives

$$\frac{\partial c_{m\lambda}}{\partial t} + v_m \frac{\partial c_{m\lambda}}{\partial z} + v_{fm} \frac{\partial c_{m\lambda}}{\partial x} = D_m^* \frac{\partial^2 c_{m\lambda}}{\partial x^2}, \quad (8)$$

where

$v_m = \dfrac{q_m}{\phi_m S_m R_m}$ is the advective transport velocity in the matrix in the z direction.

2.2. Boundary Conditions

[29] The boundary condition in fracture is

$$\lim_{z \to -\infty} c_{f\lambda}(z, t) = 0. \quad (9)$$

This is a result of the fact that no tracer can exist for $z < v_m t$, provided an initial source at $z = 0$.

[30] The boundary condition for solute transport in the rock matrix at the fracture interface is that the solute concentrations in the fracture and matrix are equal, or

$$c_{m\lambda}(0,z,t) = c_{f\lambda}(z,t). \tag{10}$$

Given a semi-infinite domain for the rock matrix,

$$\lim_{x\longrightarrow\infty} c_{m\lambda}(x,z,t) = 0, \tag{11}$$

which assigns a solute concentration of zero as $x \rightarrow \infty$.

2.3. Initial Condition

[31] The initial condition is an instantaneous point source represented as a delta function

$$c_{f\lambda}(z,0) = \frac{M_0}{A_f \phi_f S_{f0} R_f}\delta(z), \tag{12}$$

where S_{f0} is the fracture water saturation at $z = 0$, A_f is the fracture cross-sectional area orthogonal to the z axis, M_0 is the initial mass of solute (including solute sorbed), and $\delta(z)$ is the delta function.

[32] This initial condition is defined to ensure the following total solute mass condition,

$$A_f \phi_f S_{f0} R_f \int_{-\infty}^{\infty} c_{f\lambda}(z,0)dz = M_0. \tag{13}$$

The initial condition for solute mass in the rock matrix is

$$c_{m\lambda}(x,z,0) = 0, \tag{14}$$

because the solute is initially released to the fracture.

2.4. Transformation to a Moving Coordinate System

[33] The problem is transformed to a moving coordinate system to reduce the two-dimensional matrix transport problem to one spatial dimension through the following coordinate transformation,

$$\varsigma = z - v_m t. \tag{15}$$

Using equation (15), equation (5) becomes

$$\frac{\partial c_{f\lambda}}{\partial t} + v_f^* \frac{\partial c_{f\lambda}}{\partial \varsigma} = \left(\frac{2A_r}{b}\right)\left(\frac{\phi_m S_m R_m}{\phi_f S_f R_f}\right)\left(D_m^* \frac{\partial c_{m\lambda}}{\partial x}\bigg|_{x=0}\right), \tag{16}$$

where $v^*_f = v_f - v_m$ is the longitudinal velocity in the fracture relative to the matrix.

[34] The boundary and initial conditions, equations (9) and (12), for the fracture become, respectively,

$$\lim_{\varsigma\longrightarrow-\infty} c_{f\lambda}(\varsigma,t) = 0 \tag{17}$$

$$c_{f\lambda}(\varsigma,0) = \frac{M_0}{A_f \phi_f S_{f0} R_f}\delta(\varsigma). \tag{18}$$

Equation (8) for mass conservation in the matrix becomes under this transformation

$$\frac{\partial c_{m\lambda}}{\partial t} + v_{fm}\frac{\partial c_{m\lambda}}{\partial x} = D_m^* \frac{\partial^2 c_{m\lambda}}{\partial x^2}. \tag{19}$$

[35] The boundary and initial conditions for the matrix as given in equations (10), (11), and (14) become, respectively,

$$c_{m\lambda}(0,\varsigma,t) = c_{f\lambda}(\varsigma,t) \tag{20}$$

$$\lim_{x\longrightarrow\infty} c_{m\lambda}(x,\varsigma,t) = 0 \tag{21}$$

$$c_{m\lambda}(x,\varsigma,0) = 0. \tag{22}$$

Note that the multidimensional advective transport in the matrix as expressed in equation (8) is now reduced to a single spatial dimension in the transverse direction in equation (19).

2.5. Transformation to Dimensionless Form

[36] The collection of terms found on the right-hand side of equation (16) is a convenient length scale, ℓ, for the development of nondimensional variables

$$\ell = \frac{b}{2A_r}\frac{\phi_f S_f R_f}{\phi_m S_m R_m}. \tag{23}$$

This length scale represents an effective fracture water volume divided by the corresponding effective matrix water area in contact with the fracture water (see also equation (2)). The length scale also accounts for the effects of sorption through the retardation factors, which represent additional solute storage resulting from sorption. The assumption that the area reduction factor, A_r, equals the fracture saturation, S_f, leads to a constant value for the length scale, ℓ.

[37] With this length scale, the following dimensionless variables may be defined:

$$\tau = \frac{v_f^* t}{\ell} \tag{24}$$

$$\xi = \frac{\varsigma}{\ell} \tag{25}$$

$$\eta = \frac{x}{\ell} \tag{26}$$

$$c_{fd} = \frac{A_f \phi_f S_{f0} R_f \ell}{M_0} c_{f\lambda} \tag{27}$$

$$c_{md} = \frac{A_f \phi_f S_{f0} R_f \ell}{M_0} c_{m\lambda}. \tag{28}$$

[38] Using these dimensionless variables, equation (16) becomes

$$\frac{\partial c_{fd}}{\partial \tau} + \frac{\partial c_{fd}}{\partial \xi} = \frac{1}{Pe}\frac{\partial c_{md}}{\partial \eta}\bigg|_{\eta=0}, \tag{29}$$

where

$$Pe = \frac{v_f^* \ell}{D_m^*} \tag{30}$$

is the Peclet number and

$$V = \frac{v_{fm}}{v_f^*} \tag{31}$$

is the cross-flow velocity ratio. The boundary and initial conditions for the fracture, equations (17) and (18), respectively, become

$$\lim_{\xi \longrightarrow -\infty} c_{fd}(\xi, \tau) = 0 \tag{32}$$

$$c_{fd}(\xi, 0) = \delta(\xi). \tag{33}$$

Note that the nondimensional delta function in equation (33) is related to the delta function in equation (17) through the following total mass condition at $t = 0$:

$$\int_{-\infty}^{\infty} \delta(\xi) d\xi = \int_{-\infty}^{\infty} \frac{1}{\ell} \delta(\xi) dz = \int_{-\infty}^{\infty} \delta(z) dz \;\; \therefore \delta(\xi) = \ell \delta(z). \tag{34}$$

[39] Using the nondimensional variables, equation (19) becomes

$$\frac{\partial c_{md}}{\partial \tau} + V \frac{\partial c_{md}}{\partial \eta} = \frac{1}{Pe} \frac{\partial^2 c_{md}}{\partial \eta^2}. \tag{35}$$

[40] The nondimensional forms for the boundary and conditions in equations (20), (21), and (22) are, respectively,

$$c_{md}(0, \xi, \tau) = c_{fd}(\xi, \tau) \tag{36}$$

$$\lim_{\eta \longrightarrow \infty} c_{md}(\eta, \xi, \tau) = 0 \tag{37}$$

$$c_{md}(\eta, \xi, 0) = 0. \tag{38}$$

The mathematical solution of the coupled transport equations (29) and (35), subject to boundary and initial conditions given in equations (32), (33), (36), (37), and (38), is presented in the next section.

3. Mathematical Solution

3.1. Solution for the Laplace Transformed Matrix and Fracture Concentrations in the Fracture and Connected Matrix

[41] The Laplace transform may be represented as the following integral change of variables

$$H(\tau) c_{md}(\eta, \xi, \tau) = \frac{1}{2\pi i} \int_{c-i\infty}^{c+i\infty} \hat{c}_{md}(\eta, \xi, s) e^{s\tau} ds \tag{39}$$

$$H(\tau) c_{fd}(\xi, \tau) = \frac{1}{2\pi i} \int_{c-i\infty}^{c+i\infty} \hat{c}_{fd}(\xi, s) e^{s\tau} ds, \tag{40}$$

where $H(\tau)$ is the Heaviside step function defined by

$$\begin{aligned} H(\tau) &= 0; \tau < 0 \\ H(0) &= \frac{1}{2} \\ H(\tau) &= 1; \tau > 0. \end{aligned} \tag{41}$$

[42] Substituting equation (39) for c_{md} in equation (35) leads to the following differential equation in terms of $\hat{c}_{md}$:

$$\frac{d^2 \hat{c}_{md}}{d\eta^2} - PeV \frac{d\hat{c}_{md}}{d\eta} - sPe\hat{c}_{md} = 0. \tag{42}$$

The solution to equation (42) that is consistent with the transformed initial and boundary conditions from equations (37) and (38) is

$$\hat{c}_{md}(\eta, \xi, s) = \hat{c}_{fd}(\xi, s) \exp\left[\left(\frac{PeV}{2} - \sqrt{\left(\frac{PeV}{2}\right)^2 + sPe} \right) \eta \right]. \tag{43}$$

[43] The fracture solute mass conservation equation, given in equation (29), becomes the following using equations (39) and (40) subject to the initial condition in equation (33)

$$\frac{\partial \hat{c}_{fd}}{\partial \xi} + s\hat{c}_{fd} - \frac{1}{Pe} \frac{\partial \hat{c}_{md}}{\partial \eta}\bigg|_{\eta=0} = \delta(\xi). \tag{44}$$

Substituting equation (43) for $\hat{c}_{md}$ into equation (44) gives

$$\frac{d\hat{c}_{fd}}{d\xi} + \left\{ s - \frac{V}{2} + \sqrt{\frac{V^2}{4} + \frac{s}{Pe}} \right\} \hat{c}_{fd} = \delta(\xi). \tag{45}$$

Integrating equation (45) from $-\infty$ to ξ and using equation (32) gives

$$\hat{c}_{fd}(\xi, s) = \exp\left[-\left(s - \frac{V}{2} + \sqrt{\frac{V^2}{4} + \frac{s}{Pe}} \right) \xi \right] H(\xi). \tag{46}$$

Inversion of the Laplace-transformed solutions, equations (43) and (46), to physical time is presented in section 3.2.

3.2. Inversion of the Laplace Transformed Solutions for the Fracture and Connected Matrix

[44] The convolution theorem is used to simplify the dependence on s in equation (46). The convolution theorem states

$$\int_0^{\tau} F_1(\tau - \sigma) F_2(\sigma) d\sigma = \frac{1}{2\pi i} \int_{c-i\infty}^{c+i\infty} f_1(s) f_2(s) e^{s\tau} ds. \tag{47}$$

Let

$$f_1(s) = e^{-s\xi}, \tag{48}$$

which implies

$$F_1(\tau) = \delta(\tau - \xi), \tag{49}$$

and let

$$f_2(s) = \exp\left[\left(\frac{V}{2} - \sqrt{\frac{V^2}{4} + \frac{s}{Pe}}\right)\xi\right] H(\xi), \tag{50}$$

so that

$$F_2(\tau) = \frac{1}{2\pi i}\int_{c-i\infty}^{c+i\infty} H(\xi)\exp\left[\left(\frac{V}{2} - \frac{1}{\sqrt{Pe}}\sqrt{\frac{PeV^2}{4} + s}\right)\xi + s\tau\right] ds. \tag{51}$$

To evaluate F_2, let

$$\chi = s + \frac{PeV^2}{4}. \tag{52}$$

Substituting equation (52) into (51) gives

$$F_2(\tau) = H(\xi)\exp\left[\frac{V\xi}{2} - \frac{PeV^2\tau}{4}\right]\frac{1}{2\pi i} \cdot \int_{c+\frac{PeV^2}{4}-i\infty}^{c+\frac{PeV^2}{4}i\infty} \exp\left[-\frac{\xi\sqrt{\chi}}{\sqrt{Pe}} + \chi\tau\right] d\chi, \tag{53}$$

which is tabulated to give [*Abramowitz and Stegun*, 1972, equation 29.3.82]

$$F_2(\tau) = H(\xi)\exp\left[\frac{V\xi}{2} - \frac{PeV^2\tau}{4}\right]\left(\frac{\xi}{2\sqrt{\pi}\sqrt{Pe}\tau^{3/2}}\right)\exp\left[\frac{-\xi^2}{4Pe\tau}\right]. \tag{54}$$

Integrating equation (47) using equations (49) and (54) and using the definition of $\hat{c}_{fd}$ in equation (40) and integrating gives

$$c_{fd}(\xi,\tau) = H(\xi)H(\tau-\xi)\left(\frac{\xi}{2\sqrt{\pi}\sqrt{Pe}(\tau-\xi)^{3/2}}\right) \cdot \exp\left[-\left\{\frac{\xi - PeV(\tau-\xi)}{2\sqrt{Pe}\sqrt{\tau-\xi}}\right\}^2\right]. \tag{55}$$

[45] The dimensionless fracture concentration is a function of the dimensionless longitudinal position, dimensionless time, Peclet number and cross-flow velocity ratio. To obtain the solution for the matrix concentration, substitute equation (46) into equation (43) to give

$$\hat{c}_{md}(\eta,\xi,s) = H(\xi)\exp\left[-\left(s - \frac{V}{2} + \sqrt{\frac{V^2}{4} + \frac{s}{Pe}}\right)\xi\right] \cdot \exp\left[\left(\frac{PeV}{2} - \sqrt{\left(\frac{PeV}{2}\right)^2 + sPe}\right)\eta\right], \tag{56}$$

which upon rearranging, gives

$$\hat{c}_{md}(\eta,\xi,s) = H(\xi)\exp\left[\frac{V}{2}(\xi + Pe\eta)\right]\exp(-s\xi) \cdot \exp\left[-\left(\frac{\xi}{\sqrt{Pe}} + \sqrt{Pe}\eta\right)\sqrt{\frac{PeV^2}{4} + s}\right]. \tag{57}$$

[46] Following a similar series of steps as performed for the inversion of the fracture concentration using the convolution theorem, the solution for the matrix concentration is found to be

$$c_{md}(\eta,\xi,\tau) = H(\xi)H(\tau-\xi)\frac{(\xi + Pe\eta)}{2\sqrt{\pi}\sqrt{Pe}(\tau-\xi)^{3/2}} \cdot \exp\left[-\left\{\frac{\xi + Pe\eta - PeV(\tau-\xi)}{2\sqrt{Pe}\sqrt{\tau-\xi}}\right\}^2\right]. \tag{58}$$

The dimensionless matrix concentration is a function of the dimensionless transverse position in addition to the other factors that affect the dimensionless fracture concentration.

3.3. Solute Concentration in the Isolated Matrix

[47] The solution for matrix concentration in section 3.2 is for matrix in contact with fracture water and solute. However, the steady state flow pattern leads to a reduction in fracture saturation and therefore a reduction in the fracture-matrix interface area with increasing depth. The vertical movement of solute in the matrix results in a portion of the solute moving from matrix that has a wetted interface with the fracture to matrix that does not have a wetted interface (Figure 2). The region of the matrix that does not have a wetted interface is referred to as the isolated matrix because it is isolated from water and solute exchange with the fracture.

[48] First, consider the change in fracture saturation with depth. From equation (4)

$$\frac{dq_f}{dz} = -\frac{2A_r q_{fm}}{b}. \tag{59}$$

The fracture flux and area reduction are

$$q_f = K_f S_f \tag{60}$$

$$A_r = S_f. \tag{61}$$

Then, equation (59) becomes

$$\frac{dS_f}{dz} = -\frac{2q_{fm}}{bK_f}S_f. \tag{62}$$

Integrating equation (62) gives

$$\frac{S_f}{S_{f0}} = \exp\left(-\frac{2q_{fm}}{bK_f}z\right). \tag{63}$$

[49] Using the definitions of v_{fm}, v_f, ℓ, and V, from the analysis of concentrations from a fracture source, and introducing

$$\zeta = \frac{z}{\ell}$$

$$V_\ell = \frac{v_m}{v_f}$$

gives

$$\frac{S_f}{S_{f0}} = \exp[-V(1-V_\ell)\zeta]. \tag{64}$$

Therefore

$$A_r = S_{f0}\exp[-V(1-V_\ell)\zeta]. \tag{65}$$

Because solute in the isolated matrix advects downward at a constant velocity

$$t_c = t - \frac{z - z_c}{v_m}, \tag{66}$$

where z_c is the vertical coordinate at which solute enters the isolated matrix (see Figure 2) and t_c is the time at which solute enters the isolated matrix. Expressing equation (66) in terms of nondimensional variables gives

$$\tau_c(\xi, \zeta_c) = \left(\frac{1 - V_\ell}{V_\ell}\right)(\zeta_c - \xi). \tag{67}$$

[50] Equation (6) governing transport in the matrix becomes, for the isolated matrix

$$\phi_m S_m \left(\frac{\partial c_{mi}}{\partial t} + \lambda c_{mi}\right) + \rho_{bm}\left(\frac{\partial c_{mai}}{\partial t} + \lambda c_{mai}\right) + q_m \frac{\partial c_{mi}}{\partial z} = \phi_m S_m D_m \frac{\partial^2 c_{mi}}{\partial x^2}, \tag{68}$$

where the subscript i refers to the isolated matrix. After transforming into the moving coordinate system (section 2.4) and using the previously defined nondimensional variables, equation (68) becomes

$$\frac{\partial c_{mdi}}{\partial \tau} = \frac{1}{Pe}\frac{\partial^2 c_{mdi}}{\partial \eta^2}. \tag{69}$$

[51] Thus, in the moving coordinate system, solute transport in the isolated matrix is governed by a diffusion process. The concentration patterns may be evaluated using the superposition method, starting with equation (58) as the initial profile. Let τ_c be the dimensionless time for entering the isolated matrix and ξ_c be the corresponding vertical coordinate in the moving reference frame upon entering the isolated matrix. Because longitudinal transport after entering the isolated matrix is restricted to advection at the velocity v_m, ξ remains identically equal to ξ_c. The profile evolves over time through diffusion in the η dimension and advection in the ξ dimension. The solution to equation (69) for a source at time τ_c is

$$c_{mdi}(\eta, \xi, \tau_c, \tau) = \int_0^\infty \frac{\sqrt{Pe}\, c_{md}(\chi, \xi, \tau_c)\, d\chi}{\sqrt{4\pi(\tau - \tau_c)}} \exp\left[\frac{-Pe(\eta - \chi)^2}{4(\tau - \tau_c)}\right] d\chi, \tag{70}$$

where $c_{md}(\chi, \xi, \tau_c)$ is given in equation (58).

[52] The superposition solution is

$$c_{mdi}(\eta, \xi, \tau_c, \tau) = \int_0^\infty \frac{\sqrt{Pe}\, c_{md}(\chi, \xi, \tau_c)}{\sqrt{4\pi(\tau - \tau_c)}} \exp\left[\frac{-Pe(\eta - \chi)^2}{4(\tau - \tau_c)}\right] d\chi. \tag{71}$$

Substituting for $c_{md}(\chi, \xi_c, \tau_c)$ from equation (58) gives

$$c_{mdi}(\eta, \xi, \tau_c, \tau) = \int_0^\infty \frac{H(\xi_c)H(\tau_c - \xi)}{4\pi\sqrt{(\tau - \tau_c)}} \frac{(\xi + Pe\chi)}{(\tau_c - \xi)^{3/2}} \cdot \exp\left[-\left\{\frac{\xi + Pe\chi - PeV(\tau_c - \xi)}{2\sqrt{Pe}\sqrt{\tau_c - \xi}}\right\}^2\right] \cdot \exp\left[\frac{-Pe(\eta - \chi)^2}{4(\tau - \tau_c)}\right] d\chi. \tag{72}$$

[53] Performing the integration gives

$$c_{mdi}(\eta, \xi, \tau_c, \tau) = \frac{H(\xi)H(\tau_c - \xi)}{2\pi\sqrt{Pe}\sqrt{\tau - \xi}(\tau_c - \xi)} \cdot \exp\left[-\frac{\{\xi + Pe\eta - PeV(\tau_c - \xi)\}^2}{4Pe(\tau - \xi)}\right] \cdot \left\{\begin{array}{l} \frac{\sqrt{\pi}}{2}\left(\xi - \frac{\{\xi(\tau - \tau_c) - Pe\eta(\tau_c - \xi) - PeV(\tau - \tau_c)(\tau_c - \xi)\}}{\tau - \xi}\right) \\ \bullet\ \mathrm{erfc}\left[\frac{\xi(\tau - \tau_c) - Pe\eta(\tau_c - \xi) - PeV(\tau - \tau_c)(\tau_c - \xi)}{2\sqrt{Pe}\sqrt{\tau - \xi}\sqrt{\tau - \tau_c}\sqrt{\tau_c - \xi}}\right] \\ + \frac{\sqrt{Pe}\sqrt{\tau_c - \xi}\sqrt{\tau - \tau_c}}{\sqrt{\tau - \xi}} \\ \bullet \exp\left[-\frac{\{\xi(\tau - \tau_c) - Pe\eta(\tau_c - \xi) - PeV(\tau - \tau_c)(\tau_c - \xi)\}^2}{4Pe(\tau - \xi)(\tau - \tau_c)(\tau_c - \xi)}\right] \end{array}\right\}, \tag{73}$$

where $\tau_c(\xi, \zeta_c)$ is defined in equation (67). Equation (73) is equal to the concentrations in the connected matrix, as given in equation (58), as $\tau \rightarrow \tau_c$.

3.4. Cumulative Mass Arrivals in the Fracture and Connected Matrix at a Fixed Downstream Location

[54] The description of transport from an instantaneous source is often represented as a breakthrough curve, which gives the cumulative mass arrival at some point downstream of the source relative to the total mass release. Mathematically, this is the time integral of the mass flux at the downstream location divided by the total source mass.

[55] For the fracture, the integrated mass flux over time at a fixed downstream (exit) position, z_e, is

$$M_f(T) = \int_0^T A_f \phi_f S_f R_f v_f c_f(z_e, t) dt, \tag{74}$$

where T is the time of observation. Using the definition of the dimensionless concentration in equation (27), the cumulative mass integral becomes

$$\frac{M_f}{M_0}(T) = \frac{S_f}{S_{f0}} \int_0^T c_{fd}(z_e, t) \exp\left\{-\left(\frac{\lambda \ell}{v_f}\right)\left(\frac{v_f t}{\ell}\right)\right\} d\left(\frac{v_f t}{\ell}\right). \tag{75}$$

[56] Define the following dimensionless variables

$$\sigma = \frac{v_f t}{\ell} \tag{76}$$

$$\psi = \frac{v_f T}{\ell} \tag{77}$$

$$\lambda_d = \frac{\lambda \ell}{v_f}. \tag{78}$$

[57] Also, using the definition of ξ (see equations (15) and (25)), define the following variables:

$$\xi_e = \zeta_e - V_\ell \sigma, \tag{79}$$

such that $\tau - \xi_e = \sigma - \zeta_e$ where

$$\zeta_e = \frac{z_e}{\ell} \tag{80}$$

is the dimensionless downstream boundary coordinate and

$$V_\ell = \frac{v_m}{v_f} \tag{81}$$

is the longitudinal velocity ratio.

[58] Using equations (76), (77), (78), and (80) in equation (75) gives

$$\frac{M_f}{M_0}(\psi) = \exp[-V(1-V_\ell)\zeta] \int_0^\psi c_{fd}(\zeta_e, \sigma) \exp(-\lambda_d \sigma) d\sigma, \tag{82}$$

where $\frac{S_f}{S_{f0}}$ is given by equation (64). The integration of equation (82) using equation (55) for c_{fd} is performed using integral relationships given in Appendix A. The result is

$$\begin{aligned}
\frac{M_f}{M_0} &= \frac{\sqrt{(PeV+V_\ell)^2 + 4Pe\lambda_d} + V_\ell}{2\sqrt{(PeV+V_\ell)^2 + 4Pe\lambda_d}} \exp[-V(1-V_\ell)\zeta_e] \\
&\bullet \exp\left[\frac{\zeta_e(1-V_\ell)}{2Pe}\left\{(PeV+V_\ell) + \sqrt{(PeV+V_\ell)^2 + 4Pe\lambda_d}\right\} - \zeta_e\lambda_d\right] \\
&\bullet \operatorname{erfc}\left\{\frac{\zeta_e(1-V_\ell) + \sqrt{(PeV+V_\ell)^2 + 4Pe\lambda_d}(\psi-\zeta_e)}{2\sqrt{Pe}\sqrt{\psi-\zeta_e}}\right\} \\
&+ \frac{\sqrt{(PeV+V_\ell)^2 + 4Pe\lambda_d} - V_\ell}{2\sqrt{(PeV+V_\ell)^2 + 4Pe\lambda_d}} \exp[-V(1-V_\ell)\zeta_e] \\
&\bullet \exp\left[\frac{\zeta_e(1-V_\ell)}{2Pe}\left\{(PeV+V_\ell) - \sqrt{(PeV+V_\ell)^2 + 4Pe\lambda_d}\right\} - \zeta_e\lambda_d\right] \\
&\bullet \operatorname{erfc}\left\{\frac{\zeta_e(1-V_\ell) - \sqrt{(PeV+V_\ell)^2 + 4Pe\lambda_d}(\psi-\zeta_e)}{2\sqrt{Pe}\sqrt{\psi-\zeta_e}}\right\}
\end{aligned} \tag{83}$$

for $\zeta_e \le \psi \le \frac{\zeta_e}{V_\ell}$. For $\psi < \zeta_e$, $\frac{M_f}{M_0}(\psi) = 0$ and for $\psi > \frac{\zeta_e}{V_\ell}$, $\frac{M_f}{M_0}(\psi) = \frac{M_f}{M_0}\left(\frac{\zeta_e}{V_\ell}\right)$.

[59] Special forms of this solution for various limiting cases are given in Appendix B.

[60] The cumulative mass arrival in the connected matrix is also found by integrating the mass flux over time at a fixed position, z_e. However, in this case, the integration is also performed over the transverse direction, x, as given by

$$M_m(T) = 2\int_0^T \left(\frac{A_f A_r}{b}\right)\phi_m S_m R_m v_m \int_0^\infty c_m(x, z_e, t) dx dt. \tag{84}$$

Note that the 2 is needed to account for tracer mass on both sides of the fracture. The term $\frac{A_f A_r}{b}$ is the depth dimension (y in Figures 1 and 2).

[61] Expressing equation (67) in terms of the nondimensional variables gives

$$\frac{M_m}{M_0}(\psi) = V_\ell \exp[-V(1-V_\ell)\zeta] \int_0^\psi \int_0^\infty c_{md}(\eta, \zeta_e, \sigma) d\eta d\sigma, \tag{85}$$

where c_{md} is given by equation (58). The integration of equation (85) uses integral relationships given in Appendix A. The result is

$$\begin{aligned}
\frac{M_m}{M_0} &= \left[\frac{(PeV+V_\ell)VV_\ell + 4\lambda_d V_\ell}{4\lambda_d\sqrt{(PeV+V_\ell)^2 + 4Pe\lambda_d}} + \frac{VV_\ell}{4\lambda_d}\right] \exp[-V(1-V_\ell)\zeta_e] \\
&\bullet \exp\left[\frac{\zeta_e}{2Pe}(1-V_\ell)\left\{(PeV+V_\ell) - \sqrt{(PeV+V_\ell)^2 + 4Pe\lambda_d}\right\} - \zeta_e\lambda_d\right] \\
&\bullet \operatorname{erfc}\left(\frac{\zeta_e(1-V_\ell) - \sqrt{(PeV+V_\ell)^2 + 4Pe\lambda_d}(\psi-\zeta_e)}{2\sqrt{Pe}\sqrt{\psi-\zeta_e}}\right) \\
&- \left[\frac{(PeV+V_\ell)VV_\ell + 4\lambda_d V_\ell}{4\lambda_d\sqrt{(PeV+V_\ell)^2 + 4Pe\lambda_d}} - \frac{VV_\ell}{4\lambda_d}\right] \exp[-V(1-V_\ell)\zeta_e] \\
&\bullet \exp\left[\frac{\zeta_e}{2Pe}(1-V_\ell)\left\{(PeV+V_\ell) + \sqrt{(PeV+V_\ell)^2 + 4Pe\lambda_d}\right\} - \zeta_e\lambda_d\right] \\
&\bullet \operatorname{erfc}\left(\frac{\zeta_e(1-V_\ell) + \sqrt{(PeV+V_\ell)^2 + 4Pe\lambda_d}(\psi-\zeta_e)}{2\sqrt{Pe}\sqrt{\psi-\zeta_e}}\right) \\
&- \frac{VV_\ell \exp(-\lambda_d\psi)}{2\lambda_d} \exp[-V(1-V_\ell)\zeta_e] \\
&\cdot \operatorname{erfc}\left(\frac{\zeta_e(1-V_\ell) - (PeV+V_\ell)(\psi-\zeta_e)}{2\sqrt{Pe}\sqrt{\psi-\zeta_e}}\right)
\end{aligned} \tag{86}$$

for $\zeta_e \le \psi \le \frac{\zeta_e}{V_\ell}$. For $\psi < \zeta_e$, $\frac{M_m}{M_0}(\psi) = 0$ and for $\psi > \frac{\zeta_e}{V_\ell}$, $\frac{M_m}{M_0}(\psi) = \frac{M_m}{M_0}\left(\frac{\zeta_e}{V_\ell}\right)$.

[62] Special forms of this solution for various limiting cases are given in Appendix B.

[63] The relative cumulative mass (or fractional breakthrough) relationships in equations (83) and (86) are found to be functions of the dimensionless observation time, and also depend on the dimensionless downstream position, Peclet number, cross-flow velocity ratio, and longitudinal velocity ratio. The solutions vary between the dimensionless times of ζ_e and $\frac{\zeta_e}{V_\ell}$. These dimensionless times are the minimum and maximum dimensionless times for transport to the downstream location, corresponding to pure advective transport in the fracture and matrix, respectively.

3.5. Cumulative Mass Arrivals in the Isolated Matrix at a Fixed Downstream Location

[64] The amount of solute at a depth, z, passing from the connected region into the disconnected region (per unit depth) is

$$m_{mi}(z, T) = 2\int_{\frac{z}{v_f}}^T \int_0^\infty \phi_m S_m R_m c_m(x, z, t) dx v_m dt. \tag{87}$$

This flux moves at a uniform speed, v_m, from the position z to the bottom boundary, z_e. Therefore there is a time delay, Δ, in arriving at the bottom boundary of

$$\Delta = \frac{z_e - z}{v_m}. \tag{88}$$

[65] To put the integral in equation (87) in terms of the time of arrival at the bottom boundary, the time needs to be

incremented by the amount in equation (88). However, the time for evaluation of the concentration needs to be adjusted back by the same time delay to capture the correct concentrations flowing into the isolated matrix at position z; that is, the time variable in the concentration solution is replaced by

$$t \Rightarrow t - \left(\frac{z_e - z}{v_m}\right),$$

$$m_{mi}(z,T) = 2 \int_{\frac{z}{v_f} + \left(\frac{z_e - z}{v_m}\right)}^{T} \int_{0}^{\infty} \phi_m S_m R_m c_m \left(x, z, t - \left(\frac{z_e - z}{v_m}\right)\right) dx v_m dt. \tag{89}$$

[66] Consider solute in the matrix at a given level, z. As this solute advects downward a small distance increment Δz, a small portion of the matrix becomes disconnected. This portion is

$$-\frac{A_b}{b}\frac{dA_r}{dz}\Delta z. \tag{90}$$

This is the effective "width" for tracer mass passing from the connected matrix region to the isolated matrix at a position z.

[67] This formulation also introduces a restriction on the range of z for a given value of T. This is because

$$T \geq \frac{z}{v_f} + \left(\frac{z_e - z}{v_m}\right). \tag{91}$$

Rearranging this inequality in terms of z gives

$$\frac{z_e - v_m T}{1 - \frac{v_m}{v_f}} \leq z. \tag{92}$$

[68] Integrating equation (89) over z using the differential given in equation (90) and the lower bound for z given in equation (92) gives the cumulative mass flux,

$$\frac{M_{mi}}{M_0}(T) = \frac{2A_b}{b} \int_{\frac{z_e - v_m T}{1 - \frac{v_m}{v_f}}}^{z_e} \left(-\frac{dA_r}{dz}\right) \int_{\frac{z}{v_f} + \left(\frac{z_e - z}{v_m}\right)}^{T} \cdot \int_{0}^{\infty} \phi_m S_m R_m c_m \left(x, z, t - \left(\frac{z_e - z}{v_m}\right)\right) dx v_m dt dz. \tag{93}$$

[69] Using equation (65) for A_r and the definitions of the nondimensional variables gives

$$\frac{M_{mi}}{M_0} = V V_\ell (1 - V_\ell) \int_{\frac{\zeta_e - V_\ell \psi}{1 - V_\ell}}^{\zeta_e} \exp(-V(1 - V_\ell)\zeta) \bullet \int_{\zeta + \frac{1}{V_\ell}(\zeta_e - \zeta)}^{\psi} \exp(-\lambda_d \sigma) \int_{0}^{\infty} c_{md}\left(\eta, \zeta, \sigma - \frac{1}{V_\ell}(\zeta_e - \zeta)\right) d\eta d\sigma d\zeta. \tag{94}$$

Expressing equation (58) in terms of ζ and σ using the delayed time in equation (94) gives

$$c_{md}(\eta, \zeta, \sigma) = H(\zeta_e - V_\ell \sigma) H\left(\frac{\zeta}{V_\ell}(1 - V_\ell) - \frac{1}{V_\ell}(\zeta_e - V_\ell \sigma)\right) \bullet \frac{(\zeta_e - V_\ell \sigma + Pe\eta)}{2\sqrt{\pi}\sqrt{Pe}\left(\frac{\zeta}{V_\ell}(1 - V_\ell) - \frac{1}{V_\ell}(\zeta_e - V_\ell \sigma)\right)^{3/2}} \bullet \exp\left[-\left\{\frac{\zeta_e - V_\ell \sigma + Pe\eta - PeV\left(\frac{\zeta}{V_\ell}(1 - V_\ell) - \frac{1}{V_\ell}(\zeta_e - V_\ell \sigma)\right)}{2\sqrt{Pe}\sqrt{\frac{\zeta}{V_\ell}(1 - V_\ell) - \frac{1}{V_\ell}(\zeta_e - V_\ell \sigma)}}\right\}^2\right]. \tag{95}$$

The step functions in equation (95) are redundant given the integration limits in equation (93). The integration of equation (94) uses integral relationships given in Appendix A. The result is

$$\begin{aligned}
\frac{M_{mi}}{M_0} = & -\frac{PeVV_\ell^2}{2\lambda_d\left\{V_\ell\left(PeV - V_\ell + \sqrt{(PeV + V_\ell)^2 + 4Pe\lambda_d}\right) - 2Pe\lambda_d\right\}} \\
& \bullet \left\{\frac{4\lambda_d + V\left(PeV + V_\ell + \sqrt{(PeV + V_\ell)^2 + 4Pe\lambda_d}\right)}{\sqrt{(PeV + V_\ell)^2 + 4Pe\lambda_d}}\right\} \exp(-\lambda_d \zeta_e) \\
& \bullet \exp\left(-\zeta_e(1 - V_\ell)\left\{\frac{PeV - V_\ell + \sqrt{(PeV + V_\ell)^2 + 4Pe\lambda_d}}{2Pe}\right\}\right) \\
& \bullet \operatorname{erfc}\left[\frac{(\zeta_e - V_\ell \psi)}{2\sqrt{Pe}\sqrt{\psi - \zeta_e}} - \frac{\sqrt{(PeV + V_\ell)^2 + 4Pe\lambda_d} - V_\ell}{2\sqrt{Pe}}\sqrt{\psi - \zeta_e}\right] \\
& + \frac{\sqrt{PeV}V_\ell^2\left[\sqrt{(PeV + V_\ell)^2 + 4Pe\lambda_d} + \sqrt{PeV}\sqrt{PeV + 4V_\ell} - V_\ell\right]}{2\lambda_d\sqrt{PeV + 4V_\ell}\left[2V_\ell\left(PeV - V_\ell + \sqrt{(PeV + V_\ell)^2 + 4Pe\lambda_d}\right) - 4Pe\lambda_d\right]} \\
& \bullet \left\{\frac{4\lambda_d + V\left(PeV + V_\ell + \sqrt{(PeV + V_\ell)^2 + 4Pe\lambda_d}\right)}{\sqrt{(PeV + V_\ell)^2 + 4Pe\lambda_d}}\right\} \exp(-\lambda_d \psi) \\
& \bullet \exp\left\{-\frac{1}{2Pe}(\zeta_e - V_\ell \psi)\left[PeV + \sqrt{PeV}\sqrt{PeV + 4V_\ell}\right]\right\} \\
& \bullet \operatorname{erfc}\left(\frac{(\zeta_e - V_\ell \psi)}{2\sqrt{Pe}\sqrt{\psi - \zeta_e}} - \frac{\sqrt{V}}{2}\sqrt{PeV + 4V_\ell}\sqrt{\psi - \zeta_e}\right) \\
& - \frac{\sqrt{PeV}V_\ell^2\left[\sqrt{(PeV + V_\ell)^2 + 4Pe\lambda_d} - \sqrt{PeV}\sqrt{PeV + 4V_\ell} - V_\ell\right]}{2\lambda_d\sqrt{PeV + 4V_\ell}\left[2V_\ell\left(PeV - V_\ell + \sqrt{(PeV + V_\ell)^2 + 4Pe\lambda_d}\right) - 4Pe\lambda_d\right]} \\
& \bullet \left\{\frac{4\lambda_d + V\left(PeV + V_\ell + \sqrt{(PeV + V_\ell)^2 + 4Pe\lambda_d}\right)}{\sqrt{(PeV + V_\ell)^2 + 4Pe\lambda_d}}\right\} \exp(-\lambda_d \psi) \\
& \bullet \exp\left\{-\frac{1}{2Pe}(\zeta_e - V_\ell \psi)\left[PeV - \sqrt{PeV}\sqrt{PeV + 4V_\ell}\right]\right\} \\
& \bullet \operatorname{erfc}\left(\frac{(\zeta_e - V_\ell \psi)}{2\sqrt{Pe}\sqrt{\psi - \zeta_e}} + \frac{\sqrt{V}}{2}\sqrt{PeV + 4V_\ell}\sqrt{\psi - \zeta_e}\right) \\
& + \frac{PeVV_\ell^2}{2\lambda_d\left\{V_\ell\left(PeV - V_\ell - \sqrt{(PeV + V_\ell)^2 + 4Pe\lambda_d}\right) - 2Pe\lambda_d\right\}}
\end{aligned}$$

$$\cdot\left\{\frac{4\lambda_d + V\left(PeV + V_\ell - \sqrt{(PeV+V_\ell)^2 + 4Pe\lambda_d}\right)}{\sqrt{(PeV+V_\ell)^2 + 4Pe\lambda_d}}\right\}\exp(-\lambda_d\zeta_e)$$
$$\cdot\exp\left(-\frac{\zeta_e(1-V_\ell)}{2Pe}\left\{PeV - V_\ell - \sqrt{(PeV+V_\ell)^2 + 4Pe\lambda_d}\right\}\right)$$
$$\cdot\operatorname{erfc}\left[\frac{(\zeta_e - V_\ell\psi)}{2\sqrt{Pe}\sqrt{\psi-\zeta_e}} + \frac{\sqrt{(PeV+V_\ell)^2 + 4Pe\lambda_d} + V_\ell}{2\sqrt{Pe}}\sqrt{\psi-\zeta_e}\right]$$
$$+\frac{\sqrt{PeV}V_\ell^2\left[\sqrt{(PeV+V_\ell)^2 + 4Pe\lambda_d} - \sqrt{PeV}\sqrt{PeV+4V_\ell} + V_\ell\right]}{2\lambda_d\sqrt{PeV+4V_\ell}\left[2V_\ell\left(PeV - V_\ell - \sqrt{(PeV+V_\ell)^2 + 4Pe\lambda_d}\right) - 4Pe\lambda_d\right]}$$
$$\cdot\left\{\frac{4\lambda_d + V\left(PeV + V_\ell - \sqrt{(PeV+V_\ell)^2 + 4Pe\lambda_d}\right)}{\sqrt{(PeV+V_\ell)^2 + 4Pe\lambda_d}}\right\}\exp(-\lambda_d\psi)$$
$$\cdot\exp\left\{-\frac{1}{2Pe}(\zeta_e - V_\ell\psi)\left[PeV + \sqrt{PeV}\sqrt{PeV+4V_\ell}\right]\right\}$$
$$\cdot\operatorname{erfc}\left(\frac{(\zeta_e - V_\ell\psi)}{2\sqrt{Pe}\sqrt{\psi-\zeta_e}} - \frac{\sqrt{V}}{2}\sqrt{PeV+4V_\ell}\sqrt{\psi-\zeta_e}\right)$$
$$-\frac{\sqrt{PeV}V_\ell^2\left[\sqrt{(PeV+V_\ell)^2 + 4Pe\lambda_d} + \sqrt{PeV}\sqrt{PeV+4V_\ell} + V_\ell\right]}{2\lambda_d\sqrt{PeV+4V_\ell}\left[2V_\ell\left(PeV - V_\ell - \sqrt{(PeV+V_\ell)^2 + 4Pe\lambda_d}\right) - 4Pe\lambda_d\right]}$$
$$\cdot\left\{\frac{4\lambda_d + V\left(PeV + V_\ell - \sqrt{(PeV+V_\ell)^2 + 4Pe\lambda_d}\right)}{\sqrt{(PeV+V_\ell)^2 + 4Pe\lambda_d}}\right\}\exp(-\lambda_d\psi)$$
$$\cdot\exp\left\{-\frac{1}{2Pe}(\zeta_e - V_\ell\psi)\left[PeV - \sqrt{PeV}\sqrt{PeV+4V_\ell}\right]\right\}$$
$$\cdot\operatorname{erfc}\left(\frac{(\zeta_e - V_\ell\psi)}{2\sqrt{Pe}\sqrt{\psi-\zeta_e}} + \frac{\sqrt{V}}{2}\sqrt{PeV+4V_\ell}\sqrt{\psi-\zeta_e}\right)$$
$$+\frac{VV_\ell\exp(-\lambda_d\psi)\exp\{-V\zeta_e(1-V_\ell)\}}{2\lambda_d}$$
$$\cdot\operatorname{erfc}\left[\frac{(\zeta_e - V_\ell\psi)}{2\sqrt{Pe}\sqrt{\psi-\zeta_e}} - \frac{\sqrt{PeV}}{2}\sqrt{\psi-\zeta_e}\right]$$
$$-\frac{VV_\ell\left\{\sqrt{PeV} + \sqrt{PeV+4V_\ell}\right\}\exp(-\lambda_d\psi)}{4\lambda_d\sqrt{PeV+4V_\ell}}$$
$$\cdot\exp\left\{-\frac{1}{2Pe}(\zeta_e - V_\ell\psi)\left[PeV + \sqrt{PeV}\sqrt{PeV+4V_\ell}\right]\right\}$$
$$\cdot\operatorname{erfc}\left(\frac{(\zeta_e - V_\ell\psi)}{2\sqrt{Pe}\sqrt{\psi-\zeta_e}} - \frac{\sqrt{V}\sqrt{PeV+4V_\ell}}{2}\sqrt{\psi-\zeta_e}\right)$$
$$+\frac{VV_\ell\left\{\sqrt{PeV} - \sqrt{PeV+4V_\ell}\right\}\exp(-\lambda_d\psi)}{4\lambda_d\sqrt{PeV+4V_\ell}}$$
$$\cdot\exp\left\{-\frac{1}{2Pe}(\zeta_e - V_\ell\psi)\left[PeV - \sqrt{PeV}\sqrt{PeV+4V_\ell}\right]\right\}$$
$$\cdot\operatorname{erfc}\left(\frac{(\zeta_e - V_\ell\psi)}{2\sqrt{Pe}\sqrt{\psi-\zeta_e}} + \frac{\sqrt{V}\sqrt{PeV+4V_\ell}}{2}\sqrt{\psi-\zeta_e}\right) \quad (96)$$

for $\zeta_e \le \psi \le \frac{\zeta_e}{V_\ell}$. For $\psi < \zeta_e$, $\frac{M_{mi}}{M_0}(\psi) = 0$ and for $\psi > \frac{\zeta_e}{V_\ell}$, $\frac{M_{mi}}{M_0}(\psi) = \frac{M_{mi}}{M_0}\left(\frac{\zeta_e}{V_\ell}\right)$.

[70] Special forms of this solution for various limiting cases are given in Appendix B.

[71] The relative cumulative mass in the isolated matrix varies over the same range of dimensionless time and depends on the same factors as the relative cumulative mass in the fracture and connected matrix as described in section 3.4.

Table 1. Base Case Parameters

Parameter	Value
Initial fracture flux, q_f, m/s	5×10^{-8}
Matrix flux, q_m,[a] m/s	10^{-11}
Transverse flux, q_{fm},[a] m/s	3×10^{-12}
Initial fracture saturation, S_f	0.05
Matrix saturation, S_m	0.9
Fracture porosity, ϕ_f[a]	1
Matrix porosity, ϕ_m	0.111
Fracture retardation, R_f[a]	1
Matrix retardation, R_m[a]	1
Matrix diffusion coefficient, D_m,[a] m^2/s	2×10^{-11}
Fracture aperture, b, m	0.0004
Fracture area, A_f, m^2	0.001
Longitudinal distance, z_0, m	100
Solute mass released, M_0, kg	1
Decay constant, λ, 1/s	0

[a]Different values for these parameters are noted in sections 4.2, 4.3, 4.4, and 4.5.

4. Solution Behavior

[72] Some specific cases are presented to examine the solution behavior. Base case calculations are presented in section 4.1. Table 1 presents the parameters used for the base case calculations. The model domain is 100 m in the vertical direction. The base case fracture velocity is about 32 m/yr. This gives a transport time of about 3.2 years for solute that travels exclusively in the fracture. The transport time for solute that travels exclusively in the matrix is approximately 32,000 years. The base case transverse velocity is about 30 percent of the matrix longitudinal velocity. These velocities lead to a cross-flow velocity ratio (V) of 3×10^{-5} and a longitudinal velocity ratio (V_ℓ) of 10^{-4}. The diffusion coefficient for the base case is 2×10^{-11} m^2/s, and using other parameters from Table 1 gives a Peclet number (Pe), of 100. The base case solute is stable, that is, no decay.

[73] Sensitivity calculations for four different diffusion coefficients, ranging from 2×10^{-10} m^2/s to 2×10^{-14} m^2/s are given in section 4.2. Sensitivity calculations for three flow fields with different levels of transverse flow from fracture to matrix are also given in section 4.2. One case has zero transverse flow; a second case has a transverse velocity that is about 30 percent of the matrix longitudinal velocity; and a third case where the matrix transverse and longitudinal velocities are equal. Sensitivity calculations for matrix porosity and retardation are given in section 4.3, and for fracture retardation and porosity in section 4.4. Sensitivity calculations for radioactive decay are given in section 4.5.

4.1. Fracture and Matrix Concentrations and Cumulative Arrivals for the Base Case

[74] The fractional breakthrough curves for the base case, showing contributions from the fractures, connected matrix, and isolated matrix, are presented in Figure 3. Cumulative releases at the downstream position occur early in the time period for the fractures, starting at about 100 years. The fractures contribute primarily over the period of 100 to 10,000 years. Contributions to the total breakthrough begin in the connected matrix at about 1,000 years and continue to

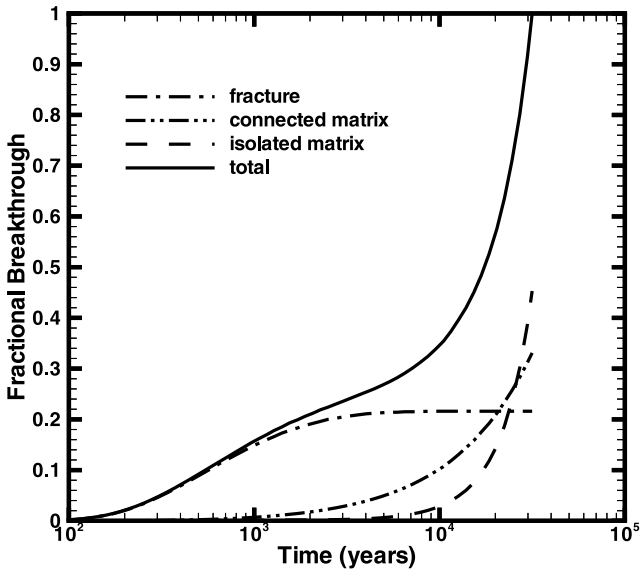

Figure 3. Base case breakthrough curves for the fracture, connected matrix, and isolated matrix. Curves were computed using equations (B1), (B2), and (B3).

contribute until all solute has exited the system at approximately 31,600 years. This is the time for solute to travel from the inlet to the outlet entirely in the matrix. Contributions from the isolated matrix are the last to arrive, at about 5,000 years, but ultimately contribute the most to the cumulative mass flux. Concentration profiles for the fractures and connected matrix are shown in Figures 4a–4c. At 50 years, very little of the solute has reached the downstream boundary. Concentrations in the connected matrix show increasing delay and decreasing concentration with distance away from the fracture. At 1,000 years, the concentrations in the connected matrix at some locations exceed the concentrations in the fracture. At 10,000 years connected matrix concentrations within 20 m of the fracture exceed the concentrations in the fracture. The sharp boundary at a longitudinal distance of about 32 m represents the matrix advection rate, which is the slowest rate for solute transport toward the bottom boundary.

[75] The change in wetted interface area with depth is shown in Figure 5. The interface area decreases from its original value at $z = 0$ to a value about 22 percent of the original at $z = 100$ m. Solute transport through the isolated matrix occurs as a result of this change in wetted interface area. Figures 6 and 7 show concentration profiles for transition depths from the connected matrix to the isolated matrix (z_c) of 10 m, 50 m, and 80 m at 1,000 years and

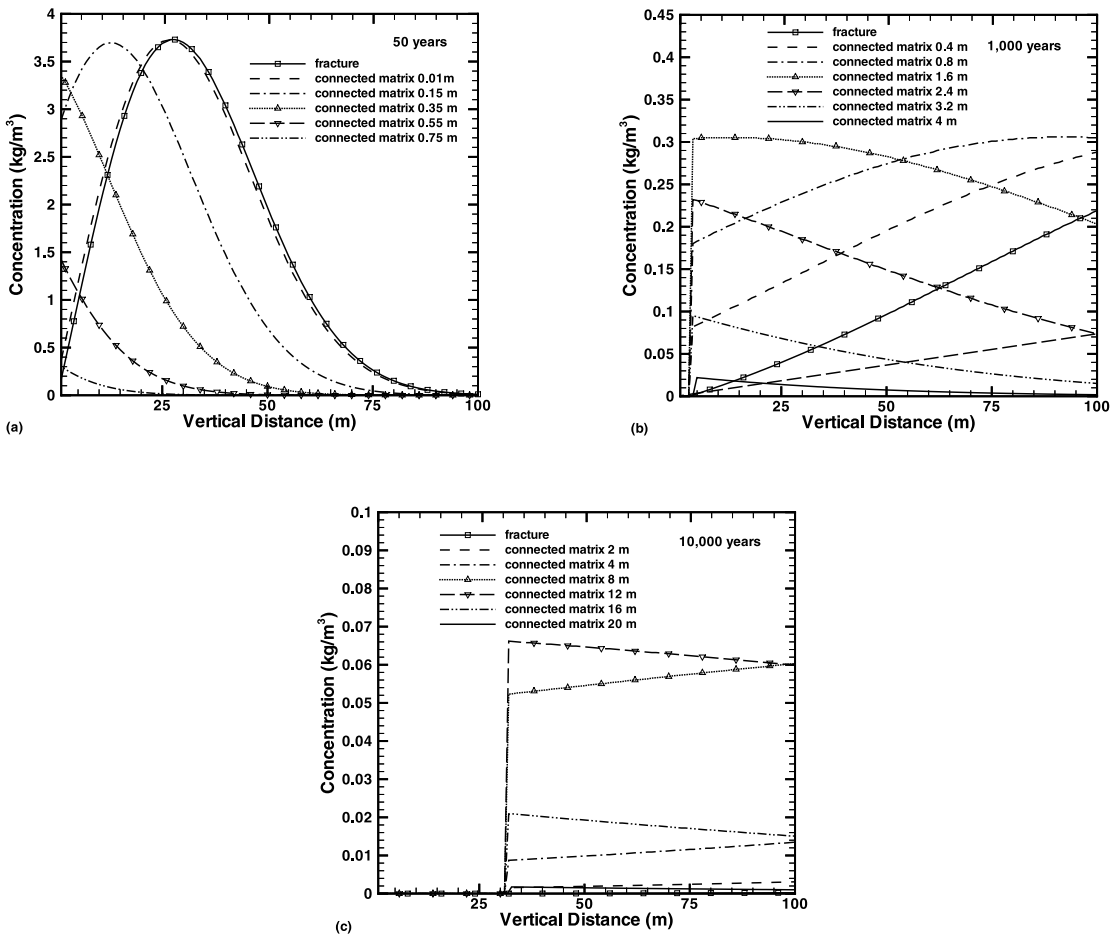

Figure 4. Base case longitudinal concentration profiles for the fracture and connected matrix: (a) 50, (b) 1000, and (c) 10,000 years. Profiles were computed using equations (55) and (58).

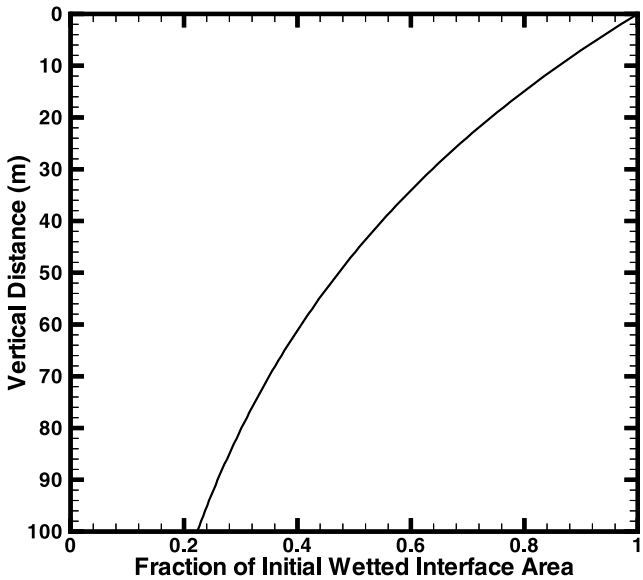

Figure 5. Fraction of wetted interface area as a function of vertical distance computed using equation (65).

10,000 years for various distances into the matrix from the fracture. Peak concentrations in the isolated matrix at 1,000 years range from about 0.7 kg/m^3 for z_c = 10 m to about 0.3 kg/m^3 for z_c = 80 m (Figures 6a–6c) as compared with peak concentrations in the connected matrix of slightly more than 0.3 kg/m^3 (Figure 4b). Peak concentrations remain higher in the isolated matrix than in the connected matrix at 10,000 years, as shown in Figures 7a–7c and 4c. This is a result of the loss of communication with the fracture, which at 1,000 years and 10,000 years has lower concentrations than in the isolated matrix near the fracture surface (depth of 0.01 m). At 1,000 years, the profiles span about 3 m longitudinally (Figures 6a–6c) and extend to more than 30 m at 10,000 years (Figures 7a–7c). The profiles stretch out with time because of the continuous solute transport from the connected matrix into the isolated matrix.

4.2. Transport Sensitivity to Matrix Diffusion, Imbibition, and Global Flow in the Matrix

[76] The magnitude and timing of cumulative mass arrivals are a function of Peclet number, *Pe*, the cross-flow velocity ratio, *V*, and the longitudinal velocity ratio, V_ℓ. The effects of variations in *Pe* are investigated through changes to the matrix diffusion coefficient. The effects of variations in *V* are investigated through changes in the imbibition flux. The effects of variations in V_ℓ are investigated through

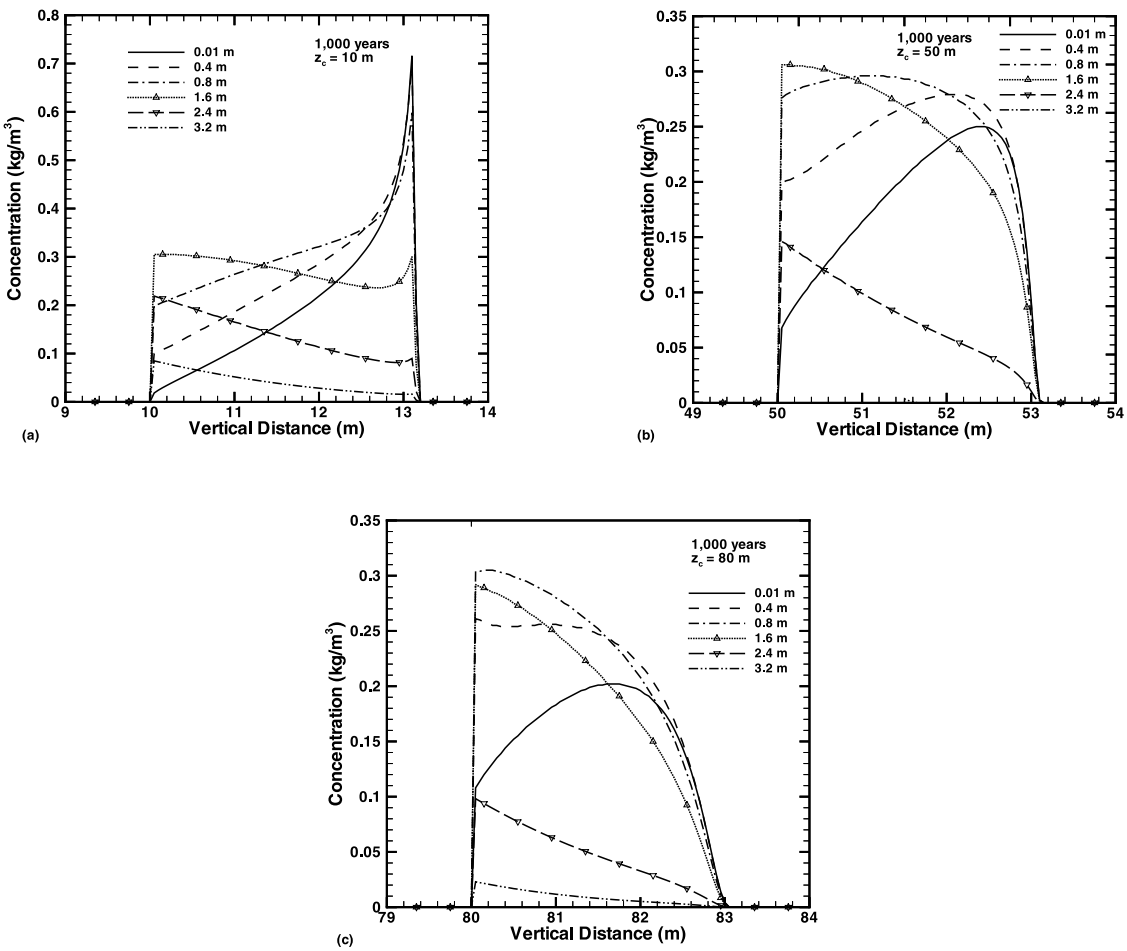

Figure 6. Base case longitudinal concentration profiles for the isolated matrix: (a) 1000 years, z_c = 10 m; (b) 1000 years, z_c = 50 m; and (c) 1000 years, z_c = 80 m. Profiles were computed using equation (73).

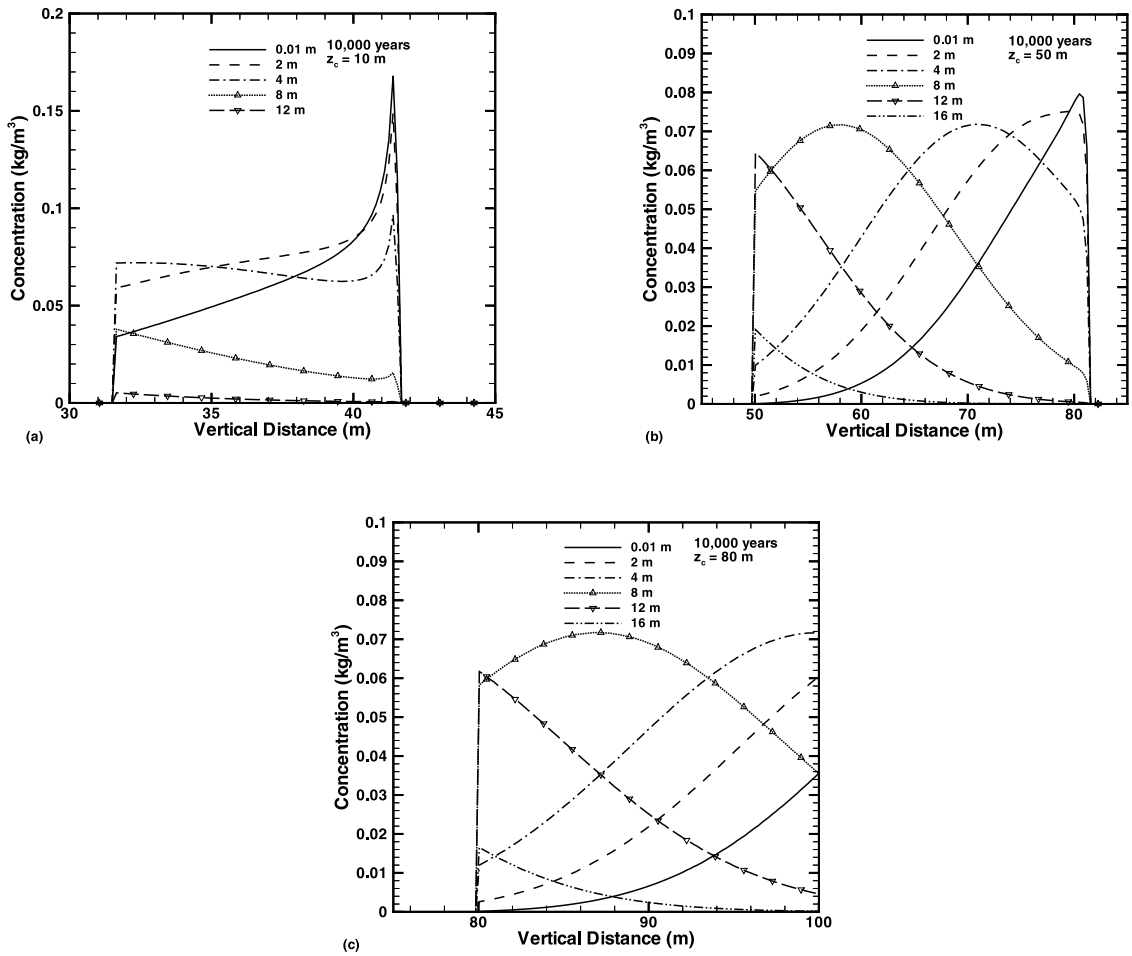

Figure 7. Base case longitudinal concentration profiles for the isolated matrix: (a) 10,000 years, $z_c = 10$ m; (b) 10,000 years, $z_c = 50$ m; and (c) 10,000 years, $z_c = 80$ m. Profiles were computed using equation (73).

changes in the matrix longitudinal flux. Parameter values for these sensitivity cases are given in Table 2.

[77] Figures 8a–8c present fractional breakthrough for all components (fracture, connected matrix, and isolated matrix) for $V_\ell = 10^{-4}$ and a range of Pe from 10 to 10,000 and a range of V from 0 to 10^{-4}. Figure 8a shows results for $V = 0$ (no transverse flow). The results show a strong sensitivity to changes in Pe, with increasingly longer breakthrough times for lower values of Pe. Figure 8b shows the behavior with a transverse velocity that is 30 percent of the matrix longitudinal velocity. The effects of transverse flow have a large impact on the breakthrough behavior at longer times, but relatively little effect on the time of first arrival. The effects of transverse flow are also greater for cases with higher values of Pe. At higher Pe, there is a distinct plateau in the fractional breakthrough curve. The level of the plateau, at a fractional breakthrough of about 0.22, corresponds to the fraction the initial flux that exits the fracture at the downstream location. This same fraction is seen in the wetted interface area at 100 m (see Figure 5), which is equivalent to the fraction of the initial water flux in the fracture. At higher transverse velocities, shown in Figure 8c, nearly all transport occurs in the matrix from the strong transverse flow, leading to low sensitivity to Pe. In this case, only about 0.0068 of the initial fracture flux exits the fracture at the downstream location.

[78] Sensitivity calculations for the case with no longitudinal transport in the matrix, $V_\ell = 0$, are shown in Figures 9a–9c. Figure 9a shows the case with $V = 0$. The loss of longitudinal advective transport in the matrix results in longer times to attain higher values of fractional breakthrough as compared with Figure 8a, with more pronounced differences at lower values of Pe. However, there is little effect on the initial breakthrough times. Figures 9b and 9c show the distinct effects of having local matrix advection from the fracture to the matrix without global longitudinal advective transport in the matrix. The fractions of solute that are ultimately produced, about 0.22 and 0.0068, respectively, correspond to the fraction of the initial fracture flux that arrives at the lower boundary. The

Table 2. Parameter Variations for Figures 8, 9, and 10

Dimensionless Variable	Parameter[a]	Value
$Pe = 10$	D_m	2×10^{-10}
$Pe = 100$	D_m	2×10^{-11}[b]
$Pe = 1{,}000$	D_m	2×10^{-12}
$Pe = 10{,}000$	D_m	2×10^{-13}
$V = 0$	q_{fm}	0
$V = 3 \times 10^{-5}$	q_{fm}	3×10^{-12}[b]
$V = 10^{-4}$	q_{fm}	10^{-11}

[a] D_m in units of m^2/s, q_{fm} in units of m/s.
[b] Base case.

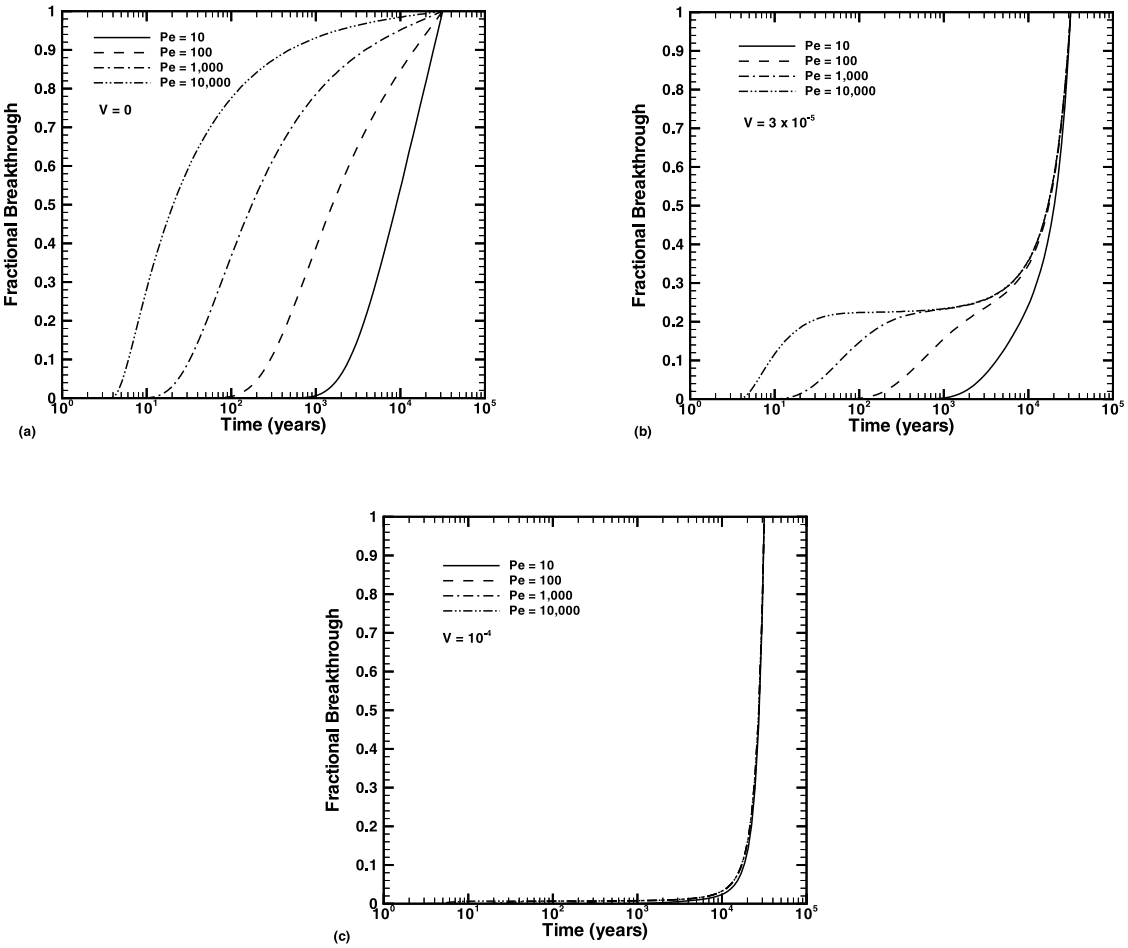

Figure 8. Effects of variations in Peclet number (*Pe*) and transverse velocity ratio (*V*) on the cumulative fractional mass breakthrough at the lower boundary: (a) $V = 0$, curves computed using equation (B7); (b) $V = 3 \times 10^{-5}$, curves computed using equation (B5); and (c) $V = 10^{-4}$, curves computed using equation (B5).

effect of *Pe* on the fractional breakthrough for these cases is restricted to the fraction of solute transport that escapes permanent loss to the matrix.

4.3. Transport Sensitivity to Matrix Retardation and Porosity

[79] Solute retardation results from sorption processes between the solute and the rock surfaces. The effects of solute retardation in the matrix for retardation factors of 1, 5, and 25 are shown in Figures 10a (*Pe* = 100) and 10b (*Pe* = 10,000). The effects of retardation result in longer times, from 31,600 years to 790,000 years, to achieve a fractional breakthrough of 1. These times are in direct proportion to the retardation factor. The breakthrough curves also show a significant effect of matrix retardation on the initial breakthrough behavior. This occurs because sorption on the matrix leads to a stronger solute concentration gradient for diffusion from the fracture to the matrix.

[80] The effects of matrix porosity on transport are shown in Figures 11a and 11b. Parameter values for these sensitivity cases are given in Table 3. Matrix porosity affects transport in two ways. Matrix porosity changes the available volume for solute transport and it also affects the effective diffusion rate. The effective matrix diffusion rate is proportional to the tortuosity of the matrix. Tortuosity is defined here as the ratio of the straight-line path length between two points to the average diffusion path length. Although the relationship between tortuosity and porosity is not unique, a simple approximation that has been proposed, when matrix porosity is less than 0.2, is to set tortuosity equal to porosity [*Liu et al.*, 2004]. In Figures 11a and 11b, two cases are presented for each change in porosity. One case changes the porosity as explicitly represented in the transport equations and the second case includes the effects on matrix diffusion. Note that even when matrix porosity does not affect the matrix diffusion rate, changes to matrix porosity lead to changes in *Pe* through the effects of matrix porosity on the length scale, ℓ. The fractional breakthrough curves are found to be sensitive to changes in matrix porosity, and have similar effects on the curves as found for matrix retardation. The fractional breakthrough curves are found to be even more sensitive to matrix porosity when the effects on matrix diffusion are included.

4.4. Transport Sensitivity to Fracture Retardation and Porosity

[81] The effects of fracture retardation and porosity are shown in Figure 12a. The results show that there is virtually no sensitivity to fracture porosity and relatively limited sensitivity to fracture retardation. Although changes in

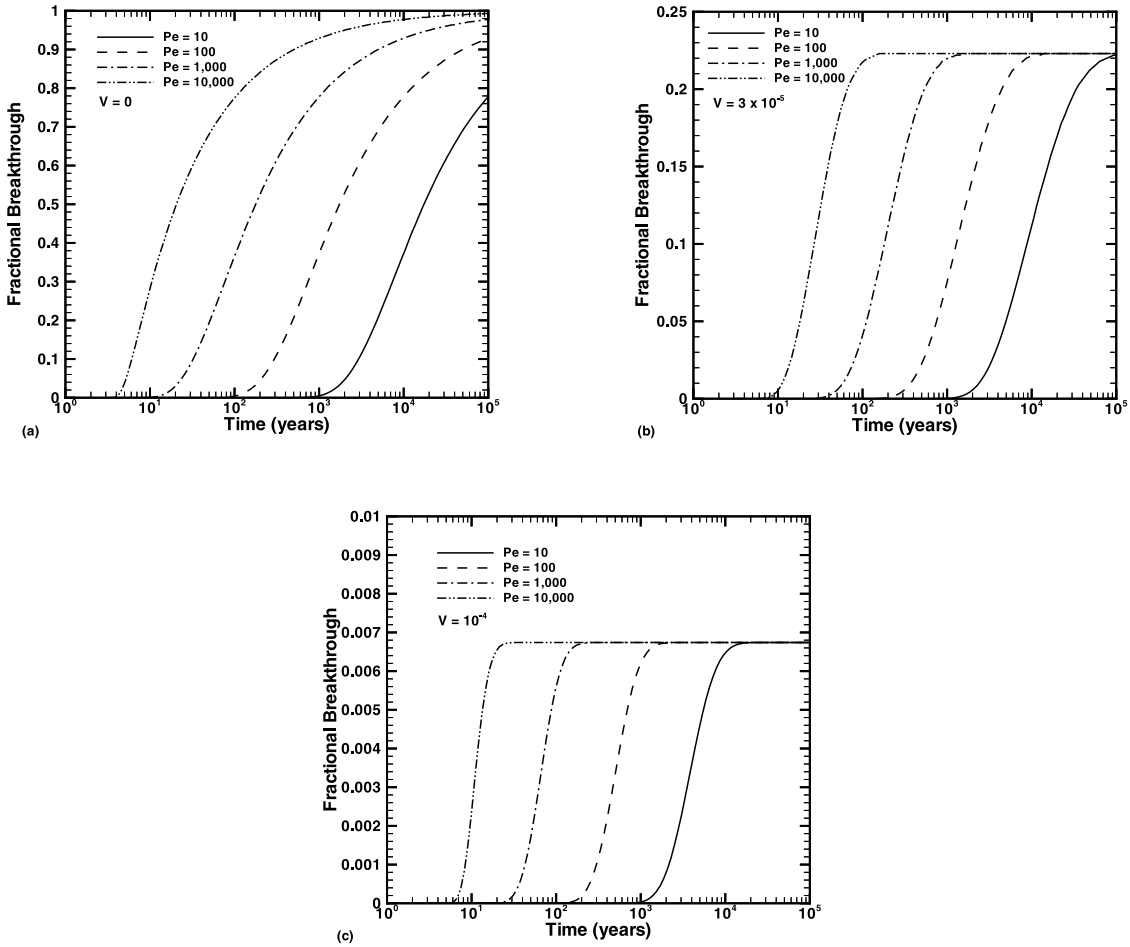

Figure 9. Effects of variations in Peclet number (*Pe*) and transverse velocity ratio (*V*) on the cumulative fractional mass breakthrough at the lower boundary for no longitudinal flow in the matrix ($V_\ell = 0$): (a) $V = 0$, curves computed using equation (B8); (b) $V = 3 \times 10^{-5}$, curves computed using equation (B6); and (c) $V = 10^{-4}$, curves computed using equation (B6).

fracture porosity and retardation directly influence the transport velocity in the fracture, they also influence the effective fracture water volume per unit fracture-matrix interface area as represented by the length scale, ℓ. For example a reduction in fracture porosity leads to higher fracture velocities if all other factors remain the same. However, the reduction in fracture porosity also leads to a smaller fracture water volume per unit fracture-matrix interface area, resulting in greater fracture-matrix interaction. The opposing effects nearly balance, resulting in low sensitivity. Increases in fracture retardation are balanced by the increase in effective fracture water volume per unit

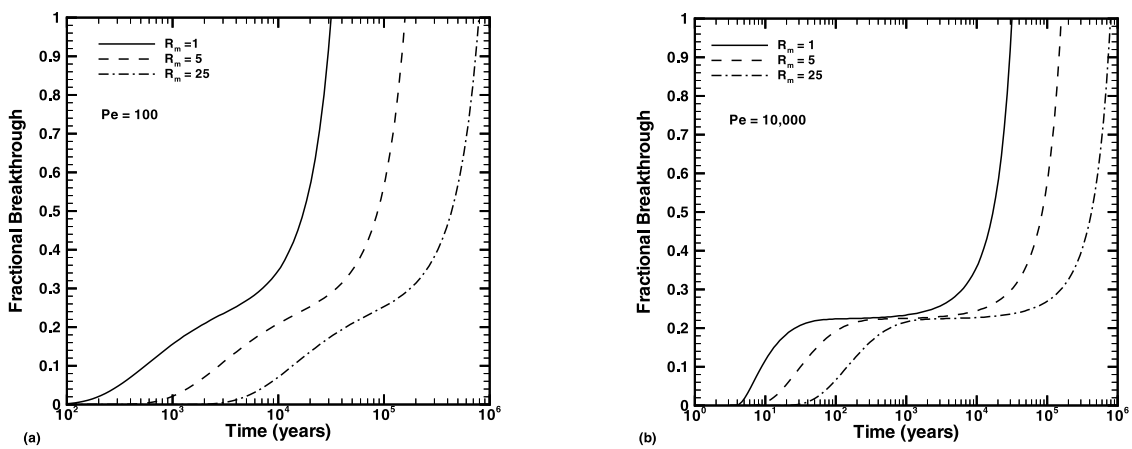

Figure 10. Effects of retardation in the matrix on the cumulative fractional mass breakthrough at the lower boundary: (a) *Pe* = 100 and (b) *Pe* = 10,000. Curves were computed using equation (B5).

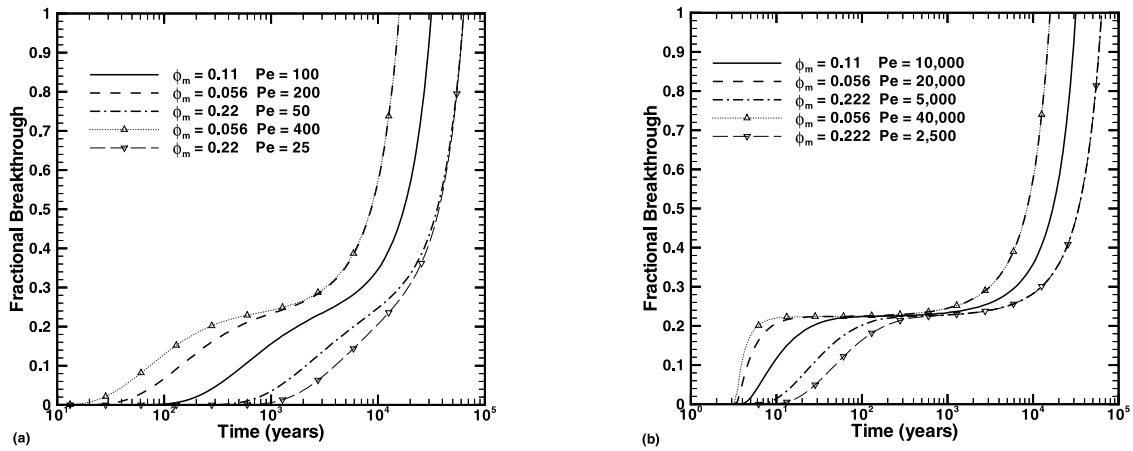

Figure 11. Effects of matrix porosity on on the cumulative fractional mass breakthrough at the lower boundary: (a) low *Pe* (effects of porosity on matrix diffusion are included in the cases with *Pe* = 400 and *Pe* = 25) and (b) high *Pe* (effects of porosity on matrix diffusion are included in the cases with *Pe* = 40,000 and *Pe* = 2500). Curves were computed using equation (B5).

fracture-matrix interface area. However, the breakthrough curve begins to be affected if the retardation level is sufficiently large to affect the relative velocity in the fracture as compared with the matrix.

[82] Figure 12b shows a case in which the matrix velocity is 90 percent of the fracture velocity for a fracture porosity of 1. Here a change in fracture porosity causes a substantial change in the breakthrough curve because the relative fracture velocity increases substantially.

[83] The fracture aperture is used to compute the fracture volume in equation (1). If the effects of fracture aperture on transport are limited to changes in fracture volume only, then the sensitivity of transport to changes in fracture aperture is equivalent to the sensitivities discussed for porosity and retardation. However, changes in fracture aperture may also affect fracture permeability. In this case, the sensitivity of transport to changes in fracture aperture is greater. The sensitivity increases because the solute velocity is affected by a change in permeability, but the effective fracture water volume per unit fracture-matrix interface area, ℓ, is not affected. For a fixed fracture-water flux, the fracture water saturation must adjust for a change in permeability. However, the change in fracture water saturation in equation (23) is exactly offset by the fracture-matrix interface area reduction factor, resulting in no change to ℓ.

4.5. Transport Sensitivity to Radioactive Decay

[84] Figure 13 shows the base case (no decay) compared with a range of radioactive half-lives. Decay has almost no effect for a half-life of 300,000 years. The total amount of material penetrating the 100 m zone is reduced by about 28 percent for a half-life of 30,000 years, which is roughly the advective timescale in the matrix. More substantial reductions are found for shorter half-lives. The amount of solute that exits the 100 m zone is reduced by about 99.9 percent for a half-life of 30 years, which is about 10 times the advective timescale in the fracture.

5. Limitations

[85] A number of specific geometric and process restrictions have been used to define the problem investigated here. Of these, the assumption of steady flow in the fracture is most likely to result in serious errors in applying the model presented here. The condition of steady flow is not always appropriate for unsaturated flow in fractured rock. Unsaturated flow is frequently linked to unsteady infiltration boundary conditions and the weak capillary forces common to unsaturated fracture flow may allow deep penetration of transient flows. In such situations, transient flow will result in faster solute transport than expected on the basis of the solutions presented here if the flow rate is assigned the time-averaged value. Transverse flow from the fracture into the matrix is represented as a constant flux in the transport model, although this is only likely to be true near the fracture; a constant transverse flow deep into the matrix is unlikely because the flow pattern is expected to disperse through the effects of rock heterogeneity and three-dimensional effects. The assumption that fracture flux is proportional to saturation is based on the formation of a gravity-driven finger structure [*Glass et al.*, 1995]. However, numerical models of flow in fractures including matrix imbibition indicate that imbibition acts to diminish the degree of instability [*Abdel-Salam and Chrysikopoulos*, 1996]. Therefore the application of this model to any particular problem requires an assessment of the model's suitability relative to the expected flow behavior.

Table 3. Parameter Variations for Figure 11

Pe	ϕ_m	D_m, m^2/s
100	0.11[a]	2×10^{-11}[a]
200	0.056	2×10^{-11}[a]
50	0.22	2×10^{-11}[a]
400[b]	0.056	10^{-11}
25[b]	0.22	4×10^{-11}
10,000	0.11[a]	2×10^{-13}
20,000	0.056	2×10^{-13}
5,000	0.22	2×10^{-13}
40,000[b]	0.056	10^{-13}
2,500[b]	0.22	4×10^{-13}

[a]Base case.
[b]Tortuosity proportional to porosity.

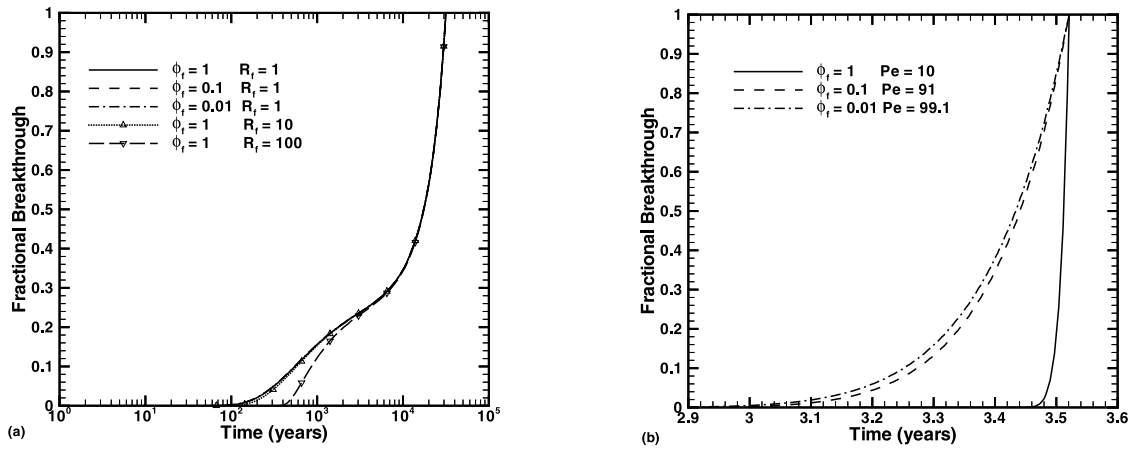

Figure 12. Effects of fracture porosity and retardation on the cumulative fractional mass breakthrough at the lower boundary: (a) base case sensitivity and (b) increased matrix flux: $q_m = 9 \times 10^{-8}$ m/s (matrix velocity 90% of fracture velocity for $\phi_f = 1$). Curves were computed using equation (B5).

[86] The concept of an isolated matrix as presented in this paper is only an approximation that is convenient for developing analytical results. The reduction in fracture-matrix interaction as fracture water saturation decreases will result in a portion of the solute in the matrix having reduced interaction with fracture water. However, no solute would be absolutely isolated from fracture water because of the presence of pathways through the matrix to fracture water.

[87] The condition of an infinite domain in the transverse direction is not appropriate when the transport is affected by the presence of multiple fractures. The analytical solutions presented here will initially be accurate if the other conditions are suitable for the problem. However, after sufficient time has elapsed for the solute to migrate laterally such that it is affected by the presence of more than one fracture, the solutions become increasingly inaccurate. The solutions can be accurate for the entire transport problem if the timescale for longitudinal transport of solute through the system is sufficiently short compared with the advective and diffusive timescales, $\frac{L_f}{v_{fm}}$ and $\frac{L_f^2}{D_m^*}$, respectively, for lateral migration between fractures separated by a distance L_f. The effects of multiple fractures have been investigated for the case where advective transport is limited to the fractures [*Sudicky and Frind*, 1982].

6. Conclusions

[88] An analytical solution is presented for transport in a single fracture through a porous rock matrix with global flow in the fracture and matrix, as well as advective and diffusive exchange between the fracture and rock matrix. The solution is derived for the concentrations that evolve from an instantaneous point source in the fracture. An integrated form of this solution for cumulative mass arrivals at a downstream location is also derived.

[89] Solute concentrations for an instantaneous release in the fracture are initially higher in the fracture, but at later times are higher in the matrix. This change is also reflected in the mass arrivals at a downstream location, which are fracture-dominated initially but dominated by solute arrivals in the matrix at later times. Solute transport in the matrix is reinforced for the case in which water is imbibing from the fracture to the matrix. This is a result of reduced fracture-matrix interface area due to a decrease in fracture water saturation as well as the direct effects of the imbibition flow pattern on solute transport back to the fracture.

[90] Sensitivity studies with the analytical model show that the solution is sensitive to changes in Peclet number, and shows increasing sensitivity to transverse flow from the fracture to the matrix with increasing Peclet number. The effects of matrix porosity and retardation are found to have a significant effect on transport behavior. These factors influence not only the matrix transport directly, but also have a significant effect on fracture-matrix interaction, affecting arrival times over the entire breakthrough curve. Sensitivity to fracture porosity and retardation are found to be small under conditions in which the fracture velocity is large relative to the matrix velocity. These factors affect

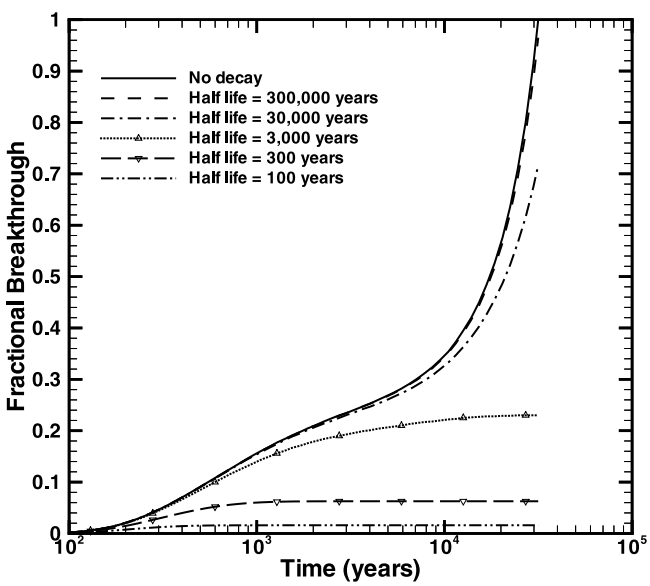

Figure 13. Effects of radioactive decay on the cumulative fractional mass breakthrough at the lower boundary. Curves were computed using equations (83), (86), and (96). The decay constant is $\lambda = 2.2 \times 10^{-8}/t_{0.5}$, where $t_{0.5}$ is the half-life in years and λ is in 1/s.

both the velocity in the fracture and fracture-water contact with the rock matrix. The opposing effects of these factors on velocity and fracture-matrix interaction for solute transport lead to the predicted low sensitivity.

Appendix A: Integral Relationships

[91] Integrations carried out for equations (83), (86), and (96) are performed using standard integration methods plus application of the following results:

$$\int \exp\left(-a^2x^2-\frac{b^2}{x^2}\right)dx=\frac{\sqrt{\pi}}{4a}\left[\exp(2ab)\operatorname{erf}\left(ax+\frac{b}{x}\right)+\exp(-2ab)\operatorname{erf}\left(ax-\frac{b}{x}\right)\right]+C \tag{A1}$$

$$\int x\exp\left(cx^2\right)\operatorname{erfc}\left(\frac{a}{x}-bx\right)dx=\frac{1}{2c}\exp\left(cx^2\right)\operatorname{erfc}\left(\frac{a}{x}-bx\right)-\left(\frac{b-\sqrt{b^2-c}}{4c\sqrt{b^2-c}}\right)\exp(2ab)\exp\left(2a\sqrt{b^2-c}\right)\operatorname{erf}\left(\frac{a}{x}+x\sqrt{b^2-c}\right)+\left(\frac{b+\sqrt{b^2-c}}{4c\sqrt{b^2-c}}\right)\exp(2ab)\exp\left(-2a\sqrt{b^2-c}\right)\cdot\operatorname{erf}\left(\frac{a}{x}-x\sqrt{b^2-c}\right)+C, \tag{A2}$$

where C is an integration constant.

Appendix B: Special Forms of the Solutions

B1. No Decay

[92] Equations (83), (87), and (96) reduce to the following for no decay ($\lambda_d = 0$). Note that for equations (86) and (96) this limit requires the first-order expansion in small λ_d.

[93] For cumulative mass in the fracture, equation (83) becomes

$$\frac{M_f}{M_0}=\frac{1}{2}\frac{PeV}{PeV+V_\ell}\exp[-V(1-V_\ell)\zeta_e]\cdot\operatorname{erfc}\left(\frac{\zeta_e(1-V_\ell)-(PeV+V_\ell)(\psi-\zeta_e)}{2\sqrt{Pe}\sqrt{\psi-\zeta_e}}\right)+\frac{1}{2}\frac{PeV+2V_\ell}{PeV+V_\ell}\exp\left[\frac{\zeta_eV_\ell(1-V_\ell)}{Pe}\right]\cdot\operatorname{erfc}\left(\frac{\zeta_e(1-V_\ell)+(PeV+V_\ell)(\psi-\zeta_e)}{2\sqrt{Pe}\sqrt{\psi-\zeta_e}}\right). \tag{B1}$$

[94] For cumulative mass in the connected matrix, equation (86) becomes

$$\frac{M_m}{M_0}=\left[\frac{(PeV+2V_\ell)V_\ell+VV_\ell(PeV+V_\ell)[(\psi-\zeta_e)(PeV+V_\ell)-\zeta_e(1-V_\ell)]}{2(PeV+V_\ell)^2}\right]\cdot\exp[-V(1-V_\ell)\zeta_e]\cdot\operatorname{erfc}\left(\frac{\zeta_e(1-V_\ell)-(PeV+V_\ell)(\psi-\zeta_e)}{2\sqrt{Pe}\sqrt{\psi-\zeta_e}}\right)-\left[\frac{(PeV+2V_\ell)V_\ell}{2(PeV+V_\ell)^2}\right]\exp\left[\frac{\zeta_eV_\ell(1-V_\ell)}{Pe}\right]\cdot\operatorname{erfc}\left(\frac{\zeta_e(1-V_\ell)+(PeV+V_\ell)(\psi-\zeta_e)}{2\sqrt{Pe}\sqrt{\psi-\zeta_e}}\right)+\left(\frac{VV_\ell\sqrt{Pe}\sqrt{\psi-\zeta_e}}{\sqrt{\pi}(PeV+V_\ell)}\right)\exp[-V(1-V_\ell)\zeta_e]\cdot\exp\left[-\left(\frac{\zeta_e(1-V_\ell)-(PeV+V_\ell)(\psi-\zeta_e)}{2\sqrt{Pe}\sqrt{\psi-\zeta_e}}\right)^2\right]. \tag{B2}$$

[95] For cumulative mass in the isolated matrix, equation (96) becomes

$$\begin{aligned}\frac{M_{mi}}{M_0}=&-\left[\frac{PeV(PeV+V_\ell)+V_\ell(PeV+2V_\ell)-\zeta_eVV_\ell(1-V_\ell)(PeV+V_\ell)-\zeta_eVV_\ell(PeV+V_\ell)^2}{2(PeV+V_\ell)^2}\right]\cdot\exp[-\zeta_eV(1-V_\ell)]\operatorname{erfc}\left(\frac{\zeta_e(1-V_\ell)-(PeV+V_\ell)(\psi-\zeta_e)}{2\sqrt{Pe}\sqrt{\psi-\zeta_e}}\right)\\&-\left[\frac{(PeV+2V_\ell)PeV}{2(PeV+V_\ell)^2}\right]\exp\left[\frac{\zeta_eV_\ell(1-V_\ell)}{Pe}\right]\cdot\operatorname{erfc}\left(\frac{\zeta_e-V_\ell\psi+(PeV+2V_\ell)(\psi-\zeta_e)}{2\sqrt{Pe}\sqrt{\psi-\zeta_e}}\right)\\&-\frac{VV_\ell\sqrt{Pe}\sqrt{\psi-\zeta_e}}{\sqrt{\pi}(PeV+V_\ell)}\exp[-\zeta_eV(1-V_\ell)]\cdot\exp\left[-\left(\frac{\zeta_e(1-V_\ell)-(PeV+V_\ell)(\psi-\zeta_e)}{2\sqrt{Pe}\sqrt{\psi-\zeta_e}}\right)^2\right]\\&+\frac{1}{2}\exp\left\{-\frac{(\zeta_e-V_\ell\psi)}{2Pe}\left[PeV+\sqrt{PeV}\sqrt{PeV+4V_\ell}\right]\right\}\cdot\operatorname{erfc}\left(\frac{\zeta_e-V_\ell\psi-\sqrt{PeV}\sqrt{PeV+4V_\ell}(\psi-\zeta_e)}{2\sqrt{Pe}\sqrt{\psi-\zeta_e}}\right)\\&+\frac{1}{2}\exp\left\{-\frac{(\zeta_e-V_\ell\psi)}{2Pe}\left[PeV-\sqrt{PeV}\sqrt{PeV+4V_\ell}\right]\right\}\cdot\operatorname{erfc}\left(\frac{\zeta_e-V_\ell\psi+\sqrt{PeV}\sqrt{PeV+4V_\ell}(\psi-\zeta_e)}{2\sqrt{Pe}\sqrt{\psi-\zeta_e}}\right)\\&-\frac{VV_\ell\exp\{-V\zeta_e(1-V_\ell)\}\psi}{2}\operatorname{erfc}\left[\frac{\zeta_e-V_\ell\psi-PeV(\psi-\zeta_e)}{2\sqrt{Pe}\sqrt{\psi-\zeta_e}}\right].\end{aligned} \tag{B3}$$

[96] Combining equations (B2) and (B3) gives the cumulative mass in the matrix for no decay,

$$\frac{M_m+M_{mi}}{M_0}=\frac{VV_\ell(PeV+V_\ell)\psi-PeV}{2(PeV+V_\ell)}\cdot\exp[-V(1-V_\ell)\zeta_e]\operatorname{erfc}\left(\frac{\zeta_e(1-V_\ell)-(PeV+V_\ell)(\psi-\zeta_e)}{2\sqrt{Pe}\sqrt{\psi-\zeta_e}}\right)-\left[\frac{(PeV+2V_\ell)V_\ell}{2(PeV+V_\ell)^2}\right]\exp\left[\frac{\zeta_eV_\ell(1-V_\ell)}{Pe}\right]\cdot\operatorname{erfc}\left(\frac{\zeta_e(1-V_\ell)+(PeV+V_\ell)(\psi-\zeta_e)}{2\sqrt{Pe}\sqrt{\psi-\zeta_e}}\right)-\left[\frac{(PeV+2V_\ell)PeV}{2(PeV+V_\ell)^2}\right]\exp\left[\frac{\zeta_eV_\ell(1-V_\ell)}{Pe}\right]\cdot\operatorname{erfc}\left(\frac{\zeta_e-V_\ell\psi+(PeV+2V_\ell)(\psi-\zeta_e)}{2\sqrt{Pe}\sqrt{\psi-\zeta_e}}\right)$$

$$+\frac{1}{2}\exp\left\{-\frac{(\zeta_e - V_\ell\psi)}{2Pe}\left[PeV + \sqrt{PeV}\sqrt{PeV + 4V_\ell}\right]\right\}$$
$$\cdot \operatorname{erfc}\left(\frac{\zeta_e - V_\ell\psi - \sqrt{PeV}\sqrt{PeV + 4V_\ell}(\psi - \zeta_e)}{2\sqrt{Pe}\sqrt{\psi - \zeta_e}}\right)$$
$$+\frac{1}{2}\exp\left\{-\frac{(\zeta_e - V_\ell\psi)}{2Pe}\left[PeV - \sqrt{PeV}\sqrt{PeV + 4V_\ell}\right]\right\}$$
$$\cdot \operatorname{erfc}\left(\frac{\zeta_e - V_\ell\psi + \sqrt{PeV}\sqrt{PeV + 4V_\ell}(\psi - \zeta_e)}{2\sqrt{Pe}\sqrt{\psi - \zeta_e}}\right)$$
$$-\frac{VV_\ell\psi}{2}\exp[-V\zeta_e(1 - V_\ell)]\operatorname{erfc}\left[\frac{\zeta_e - V_\ell\psi - PeV(\psi - \zeta_e)}{2\sqrt{Pe}\sqrt{\psi - \zeta_e}}\right]. \quad \text{(B4)}$$

[97] Combining equations (B1) and (B4) gives the total cumulative mass for no decay,

$$\frac{M_f + M_m + M_{mi}}{M_0} = \frac{VV_\ell\psi}{2}\exp[-V(1 - V_\ell)\zeta_e]$$
$$\cdot \operatorname{erfc}\left(\frac{\zeta_e(1 - V_\ell) - (PeV + V_\ell)(\psi - \zeta_e)}{2\sqrt{Pe}\sqrt{\psi - \zeta_e}}\right)$$
$$+\left[\frac{(PeV + 2V_\ell)PeV}{2(PeV + V_\ell)^2}\right]\exp\left[\frac{\zeta_e V_\ell(1 - V_\ell)}{Pe}\right]$$
$$\cdot \operatorname{erfc}\left(\frac{\zeta_e(1 - V_\ell) + (PeV + V_\ell)(\psi - \zeta_e)}{2\sqrt{Pe}\sqrt{\psi - \zeta_e}}\right)$$
$$-\left[\frac{(PeV + 2V_\ell)PeV}{2(PeV + V_\ell)^2}\right]\exp\left[\frac{\zeta_e V_\ell(1 - V_\ell)}{Pe}\right]$$
$$\cdot \operatorname{erfc}\left(\frac{\zeta_e - V_\ell\psi + (PeV + 2V_\ell)(\psi - \zeta_e)}{2\sqrt{Pe}\sqrt{\psi - \zeta_e}}\right)$$
$$+\frac{1}{2}\exp\left\{-\frac{(\zeta_e - V_\ell\psi)}{2Pe}\left[PeV + \sqrt{PeV}\sqrt{PeV + 4V_\ell}\right]\right\}$$
$$\cdot \operatorname{erfc}\left(\frac{\zeta_e - V_\ell\psi - \sqrt{PeV}\sqrt{PeV + 4V_\ell}(\psi - \zeta_e)}{2\sqrt{Pe}\sqrt{\psi - \zeta_e}}\right)$$
$$+\frac{1}{2}\exp\left\{-\frac{(\zeta_e - V_\ell\psi)}{2Pe}\left[PeV - \sqrt{PeV}\sqrt{PeV + 4V_\ell}\right]\right\}$$
$$\cdot \operatorname{erfc}\left(\frac{\zeta_e - V_\ell\psi + \sqrt{PeV}\sqrt{PeV + 4V_\ell}(\psi - \zeta_e)}{2\sqrt{Pe}\sqrt{\psi - \zeta_e}}\right)$$
$$-\frac{VV_\ell\psi}{2}\exp[-V(1 - V_\ell)\zeta_e]\operatorname{erfc}\left[\frac{\zeta_e - V_\ell\psi - PeV(\psi - \zeta_e)}{2\sqrt{Pe}\sqrt{\psi - \zeta_e}}\right]. \quad \text{(B5)}$$

B2. No Decay and No Longitudinal Flow in the Matrix

[98] Equation (B5) becomes, for no longitudinal flow in the matrix ($V_\ell = 0$)

$$\frac{M_f + M_m + M_{mi}}{M_0} = \frac{1}{2}\left\{\exp(-V\zeta_e)\operatorname{erfc}\left(\frac{\zeta_e - PeV(\psi - \zeta_e)}{2\sqrt{Pe}\sqrt{\psi} - \zeta_e}\right) + \operatorname{erfc}\left(\frac{\zeta_e + PeV(\psi - \zeta_e)}{2\sqrt{Pe}\sqrt{\psi - \zeta_e}}\right)\right\}. \quad \text{(B6)}$$

B3. No Decay and No Imbibition

[99] Equation (B5) becomes, for no imbibition ($V = 0$),

$$\frac{M_f + M_m + M_{mi}}{M_0} = \operatorname{erfc}\left(\frac{\zeta_e - V_\ell\psi}{2\sqrt{Pe}\sqrt{\psi - \zeta_e}}\right). \quad \text{(B7)}$$

B4. No Decay, No Longitudinal Flow in the Matrix, and No Imbibition

[100] Equation (B5) becomes, for no longitudinal flow in the matrix ($V_\ell = 0$) and no imbibition ($V = 0$),

$$\frac{M_f + M_m + M_{mi}}{M_0} = \operatorname{erfc}\left(\frac{\zeta_e}{2\sqrt{Pe}\sqrt{\psi - \zeta_e}}\right). \quad \text{(B8)}$$

Notation

Primary Variables

- A_f fracture cross-sectional area orthogonal to the z axis (L^2).
- A_r fracture-matrix interface area reduction factor (dimensionless).
- A_{vfm} fracture-matrix interface area/unit fracture volume (1/L).
- b fracture aperture (L).
- c_f solute mass concentration in fracture water (M/L^3).
- c_{fa} sorbed concentration; mass of sorbed solute per unit mass of rock (dimensionless).
- c_{fcs} fracture concentration field from a continuous point source (M/L^3).
- c_m solute mass concentration in connected matrix water (M/L^3).
- c_{ma} solute sorbed concentration in connected matrix expressed as mass of sorbed solute per unit mass of rock matrix (dimensionless).
- c_{mi} solute mass concentration in isolated matrix water (M/L^3).
- c_{mai} solute sorbed concentration in isolated matrix expressed as mass of sorbed solute per unit mass of rock matrix (dimensionless).
- D_m matrix diffusion coefficient (L^2/T).
- K_{df} linear sorption coefficient (L^3/M).
- K_{dm} linear sorption coefficient in the rock matrix (L^3/M).
- K_f fracture permeability (L^2).
- M_0 initial mass of solute (including solute sorbed) (M).
- q_f fracture water flux (fracture water flow rate per unit fracture area) (L/T).
- q_{fm} fracture-matrix flow rate per unit bulk area in x direction (L/T).
- q_m matrix water flow rate per unit bulk area (in z direction) (L/T).
- S_f fracture water saturation (fracture water volume per unit fracture volume) (dimensionless).
- S_{f0} fracture water saturation at $z = 0$ (fracture water volume per unit fracture volume) (dimensionless).

S_m matrix water saturation (matrix water volume per unit matrix bulk volume) (dimensionless).
t time (T).
t_c time of solute entry into isolated matrix (T).
T time of observation (T).
x horizontal coordinate (L).
z vertical coordinate (L).
z_c vertical coordinate of solute entry into isolated matrix (L).
z_e vertical coordinate of the lower boundary (L).
ϕ_f fracture porosity (fracture pore volume per unit fracture volume) (dimensionless).
ϕ_m matrix porosity (matrix pore volume per unit matrix bulk volume) (dimensionless).
λ decay constant for the radioactive solute (1/T).
ρ_{bf} rock mass available for sorption per unit fracture volume (M/L^3).
ρ_{bm} rock mass per unit bulk volume (M/L^3).

Derived Variables

$c_{fd} = \frac{A_f \phi_f S_{f0} R_f \ell}{M_0} c_{f\lambda}$ dimensionless fracture concentration from an instantaneous point source.

$c_{md} = \frac{A_f \phi_f S_{f0} R_f \ell}{M_0} c_{m\lambda}$ dimensionless connected matrix concentration from an instantaneous point source.

$c_{mdi} = \frac{A_f \phi_f S_{f0} R_f \ell}{M_0} c_{m\lambda i}$ dimensionless isolated matrix concentration from an instantaneous point source.

$c_{f\lambda} = c_f e^{\lambda t}$ fracture concentration normalized for radioactive decay.

$c_{m\lambda} = c_m e^{\lambda t}$ connected matrix concentration normalized for radioactive decay.

$c_{m\lambda i} = c_{mi} e^{\lambda t}$ isolated matrix concentration normalized for radioactive decay.

$\hat{c}_{md}$ Laplace transformed dimensionless matrix concentration.

$\hat{c}_{fd}$ Laplace transformed dimensionless fracture concentration.

$D_m^* = \frac{D_m}{R_m}$ effective matrix diffusion coefficient (L^2/T).

$\ell = \frac{b}{2A_r} \frac{\phi_f S_f R_f}{\phi_m S_m R_m}$ length scale (L).

$M_f(T)$ cumulative mass arrivals in the fracture (M).

$M_m(T)$ cumulative mass arrivals in the connected matrix (M).

$M_{mi}(T)$ cumulative mass arrivals in the isolated matrix (M).

$m_{mi}(z, T)$ cumulative mass arrivals at the boundary between the connected and isolated matrix per unit depth (M/L).

$Pe = \frac{v_f^* \ell}{D_m^*}$ Peclet number (dimensionless).

$R_f = 1 + \frac{A_r \rho_{bf} K_{df}}{\phi_f S_f}$ retardation coefficient in for transport in the fracture (dimensionless).

$R_m = 1 + \frac{\rho_{bm} K_{dm}}{\phi_m S_m}$ retardation coefficient for transport in the matrix.

s Laplace transform variable.

T time of observation (T).

$v_f = \frac{q_f}{\phi_f S_f R_f}$ advective transport velocity in the fracture (L/T).

$v_{fm} = \frac{q_{fm}}{\phi_m S_m R_m}$ advective transport velocity in the matrix (x direction) (L/T).

$v_f^* = v_f - v_m$ longitudinal velocity in the fracture relative to the matrix (L/T).

$v_m = \frac{q_m}{\phi_m S_m R_m}$ advective transport velocity in the matrix in the z direction (L/T).

$V = \frac{v_{fm}}{v_f^*}$ velocity ratio for cross flow in the matrix (dimensionless).

$V_\ell = \frac{v_m}{v_f}$ velocity ratio for longitudinal flow in the matrix (dimensionless).

$\chi = s + \frac{PeV^2}{4}$ modified Laplace transform variable (dimensionless).

$\eta = \frac{x}{\ell}$ dimensionless transverse distance.

$\lambda_d = \frac{\lambda \ell}{v_f}$ dimensionless decay rate.

$\sigma = \frac{v_f t}{\ell}$ dimensionless time.

$\varsigma = z - v_m t$ longitudinal coordinate in reference frame moving at the matrix velocity (L/T).

$\tau = \frac{v_f^* t}{\ell}$ dimensionless time in reference frame moving at the matrix velocity.

$\tau_c = \frac{v_f^* t_c}{\ell}$ dimensionless time of solute entry inot the isolated matrix in reference frame moving at the matrix velocity.

$\xi = \frac{\varsigma}{\ell}$ dimensionless longitudinal coordinate for reference frame moving at the matrix velocity.

$\xi_c = \frac{z_c - v_m t_c}{\ell}$ dimensionless longitudinal coordinate for solute entry into the isolated matrix for reference frame moving at the matrix velocity.

$\psi = \frac{v_f T}{\ell}$ dimensionless observation time.

$\zeta = \frac{z}{\ell}$, dimensionless longitudinal distance.

$\zeta_c = \frac{z_c}{\ell}$ dimensionless longitudinal distance at entry point into isolated matrix.

$\zeta_e = \frac{z_e}{\ell}$ dimensionless longitudinal distance of lower boundary.

Special Functions

$\delta(\xi)$ delta function.
$H(\xi)$ step function.

[101] **Acknowledgment.** This work was supported by the director, Office of Science, Office of Basic Energy Sciences, of the U.S. Department of Energy under contract DE-A C03-76SF00098.

References

Abdel-Salam, A., and C. V. Chrysikopoulos (1996), Unsaturated flow in a quasi-three-dimensional fractured medium with spatially variable aperture, *Water Resour. Res.*, *32*(6), 1531–1540.

Abramowitz, M., and I. A. Stegun (Eds.) (1972), *Handbook of Mathematical Functions With Formulas, Graphs, and Mathematical Tables*, *Appl. Math. Ser.*, vol. 55, 1046 pp., Natl. Bur. of Stand., U.S. Dep. of Commer., Washington, D. C.

Becker, M. W., and A. M. Shapiro (2000), Tracer transport in fractured crystalline rock: Evidence of nondiffusive breakthrough tailing, *Water Resour. Res.*, *36*(7), 1677–1686.

Bodvarsson, G. S., W. Boyle, R. Patterson, and D. Williams (1999), Overview of scientific investigations at Yucca Mountain: The potential repository for high-level nuclear waste, *J. Contam. Hydrol.*, *38*, 3–24.

Doughty, C. (1999), Investigation of conceptual and numerical approaches for evaluating moisture, gas, chemical, and heat transport in fractured unsaturated rock, *J. Contam. Hydrol.*, *38*, 69–106.

Glass, R. J., M. J. Nicholl, and V. C. Tidwell (1995), Challenging models for flow in unsaturated, fractured rock through exploration of small-scale processes, *Geophys. Res. Lett.*, *22*(11), 1457–1460.

Glass, R. J., M. J. Nicholl, A. L. Ramirez, and W. D. Daily (2002), Liquid phase structure within an unsaturated fracture network beneath a surface infiltration event: Field experiment, *Water Resour. Res.*, *38*(10), 1199, doi:10.1029/2000WR000167.

Ho, C. K. (2001), Dual-porosity vs. dual-permeability models of matrix diffusion in fractured rock, paper presented at 9th International High-Level Radioactive Waste Management Conference, Am. Nucl. Soc., Las Vegas, Nev., 29 April to 3 May.

Hughes, R. G., and M. J. Blunt (2001), Network modeling of multiphase flow in fractures, *Adv. Water Resour.*, *21*, 409–421.

Liu, H. H., C. Doughty, and G. S. Bodvarsson (1998), An active fracture model for unsaturated flow and transport in fractured rocks, *Water Resour. Res.*, *34*(10), 2633–2646.

Liu, H. H., G. S. Bodvarsson, and G. Zhang (2004), Scale dependency of the effective matrix diffusion coefficient, *Vadose Zone J.*, *3*(1), 312–315.

Maloszewski, P., and A. Zuber (1985), On the theory of tracer experiments in fissured rocks with a porous matrix, *J. Hydrol.*, *79*, 333–358.

Maloszewski, P., and A. Zuber (1990), Mathematical modeling of tracer behavior in short-term experiments in fissured rocks, *Water Resour. Res.*, *26*(7), 1517–1528.

Maloszewski, P., and A. Zuber (1992), On the calibration and validation of mathematical models for the interpretation of tracer experiments in groundwater, *Adv. Water Resour.*, *15*, 47–62.

Maloszewski, P., and A. Zuber (1993), Tracer experiments in fractured rocks: Matrix diffusion and the validity of models, *Water Resour. Res.*, *29*(8), 2723–2735.

Neretnieks, I. (1980), Diffusion in the rock matrix: An important factor in radionuclide retardation, *J. Geophys. Res.*, *85*(B8), 4379–4397.

Nicholl, M. J., R. J. Glass, and S. W. Wheatcraft (1994), Gravity-driven infiltration instability in initially dry nonhorizontal fractures, *Water Resour. Res.*, *33*(9), 2533–2546.

Pan, L., and G. S. Bodvarsson (2002), Modeling transport in fractured porous media with the random-walk particle method: The transient activity range and the particle transfer probability, *Water Resour. Res.*, *38*(6), 1080, doi:10.1029/2001WR000901.

Robinson, B. A., C. Li, and C. K. Ho (2003), Performance assessment model development and analysis of radionuclide transport in the unsaturated zone, Yucca Mountain, Nevada, *J. Contam. Hydrol.*, *62–63*, 249–268.

Shapiro, A. M. (2001), Effective matrix diffusion in kilometer-scale transport in fractured crystalline rock, *Water Resour. Res.*, *37*(3), 507–522.

Sudicky, E. A., and E. O. Frind (1982), Contaminant transport in fractured porous media: Analytical solutions for a system of parallel fractures, *Water Resour. Res.*, *18*(6), 1634–1642.

Tang, D. H., E. O. Frind, and E. A. Sudicky (1981), Contaminant transport in fractured porous media: Analytical solution for a single fracture, *Water Resour. Res.*, *17*(3), 555–564.

Zimmerman, R. W., T. Hadgu, and G. S. Bodvarsson (1996), A new lumped-parameter model for flow in unsaturated dual-porosity media, *Adv. Water Resour.*, *19*, 317–327.

J. E. Houseworth, Lawrence Berkeley National Laboratory, 1 Cyclotron Road, Berkeley, CA 94720, USA. (jehouseworth@lbl.gov)